University of Zurich[UZH]

Arctic temperature extremes increase under solar radiation management - evaluation of geoengineering effects on the Arctic climate system

ESS 510 Master's Thesis

Author
Rhonda Müller
16-726-408

Supervised by
Prof. Dr. Gabriela Schaepman
Dr. Jin-Soo Kim (jinsoo.kim@cityu.edu.hk)

Faculty representative
Prof. Dr. Gabriela Schaepman

26.08.2022
Department of Geography, University of Zurich

Abstract

Radiative forcing geoengineering (RFG) is discussed as a potential intermediate solution to partially offset greenhouse gas-driven warming by altering the Earth's energy budget. Earth system model simulations suggest that while these methods succeed at keeping the global mean temperature increase below 2°C compared to pre-industrial levels, they might lead to responses in other climate variables such as extreme temperatures. However, the Arctic region with its rapid warming and the response of extreme temperatures have not been in the focus of previous RFG studies. In the scope of this thesis, we show based on the analysis of Earth System Model simulations that RFG could exacerbate Arctic temperature extremes. The three geoengineering methods, Stratospheric Aerosol Injection, Marine Sky Brightening, and Cirrus Cloud Thinning, are simulated so that they reduce the radiative forcing from 8.5 Wm^{-2} to 4.5 Wm^{-2} by 2100. All three methods mitigate the global mean temperature rise, however, the Arctic still warms by 5°C by 2100 under RFG compared to pre-industrial temperatures. However, decreasing atmospheric CO_2 concentrations is not the aim of RFG and we show that the effect of closing plant stomata under elevated CO_2 levels is not controlled by RFG. The maximum temperature increase in the Arctic under Cirrus Cloud Thinning and Marine Sky Brightening was primarily attributed to this CO_2 plant physiological forcing, shifting the system into climatic conditions favouring fire activity. Under Stratospheric Aerosol Injection, 3.9% of the Arctic land area shifts to temperatures permanently above 0°C, exacerbating climatic conditions for permafrost thaw. This thesis concludes that there may be negative side effects of RFG such as an alteration of extreme conditions in the Arctic terrestrial systems, increasing the risk for fires, and permafrost thaw.

Contents

List of Figures

List of Tables

List of Abbreviations

BiI_3	Bismuth Triiodide
CCN	Cloud Condensation Nuclei
CCSM4	Community Climate System Model version 4
CCT	Cirrus Cloud Thinning
CDR	Carbon Dioxide Removal
CMIP5	Climate Model Intercomparison Project version 5
CO_2	Carbon Dioxide
DJF	December, January, February (boreal winter months)
ESM	Earth System Model
GeoMIP	Geoengineering Model Intercomparison Project
$GtCO_2$-eq	Gigaton Carbon Dioxide equivalent
IPCC	Intergovernmental Panel on Climate Change
JJA	June, July, August (boreal summer months)
LAI	Leaf Area Index
LR	Linear Regression
MSB	Marine Sky Brightening
NaCl	Sodium Chloride
NDC	Nationally Determined Contribution
NorESM1	Norwegian Earth System Model
RCP	Representative Concentration Pathway
RFG	Radiative Forcing Geoengineering
SAI	Stratospheric Aerosol Injection
SCoPEx	Stratospheric Controlled Perturbation Experiment
SO_2	Sulfur Dioxide
SPICE	Stratospheric Particle Injection for Climate Engineering
T_{glob}	Global Mean Temperature over Land and Ocean
T_{mean}	Mean Temperature over Land
T_{Nn}	Minimum Temperature over Land
TOA	Top of Atmosphere
T_{Xx}	Maximum Temperature over Land

Statement of Submission to a Journal

The results of the study presented in this thesis were used to prepare a manuscript that was sent to a scientific journal. The manuscript on which this thesis is based on was submitted to *Nature Communications* on the 13th of July 2022 and can be found in the version it was submitted as in the Appendix (section 7.2). The model output was kindly provided by Jerry Tjiputra[1], Helene Muri[2], and Hanna Lee[3]. The manuscript was written by myself, with comments and revisions included from all co-authors. The main ideas for the analysis were developed in collaboration with Dr. Jin-Soo Kim. The codes for the figures were all written by myself and can be found on GitHub (https://GitHub.com/RhondaMueller/Codes-RFG-Arctic-Impacts.git). I presented this work on the 28.06.2022 in an oral contribution in the "*Arctic biodiversity under global change*" session at the World Biodiversity Forum 2022.

[1]NORCE Norwegian Research Institute, Bjerknes Centre for Climate Research, Bergen, Norway
[2]Industrial Ecology Programme, Department of Energy and Process Engineering, Norwegian University of Science and Technology, Trondheim, Norway
[3]Department of Biology, Norwegian University of Science and Technology, Trondheim, Norway

1 Introduction

In the Paris Agreement of 2015, a total of 196 nations agreed to limit the global mean temperature increase to 2°C while aiming for 1.5°C (UNFCCC, 2015). For the first time, nations around the globe united to take action against climate change, which is seen by many as a milestone in the attempts to limit temperature increase on a global scale. As a legally binding treaty, the agreement aims to achieve a climate neutral world by mid-twentieth-century through economic and social transformations (UNFCCC, 2015). This would mean net zero emissions of harmful gases like carbon, methane, or nitrous oxide by 2050. This, however, requires all countries to accelerate their implementation of policies to reach the required reduction in anthropogenic carbon dioxide (CO_2) and other greenhouse gas emissions. However, it was estimated that there will be a significant emission reduction gap by 2030 (Geiges et al., 2020; Roelfsema et al., 2020), even if the Nationally Determined Contributions (NDCs) would be fulfilled by all countries (Roelfsema et al., 2020). In the latest assessment of the Intergovernmental Panel on Climate Change (IPCC), it was concluded that by 2030, CO_2 emissions should have decreased by approximately 12-46% compared to 2019 (equivalent to greenhouse gas emissions of 30-49 Gigaton CO_2 equivalent per year ($GtCO_2$-eq yr^{-1})) in order to reach the 2°C goal (Riahi et al., 2022). However, current estimates factoring in national policies assume a median emission gap by 2030 of approximately 22.4 $GtCO_2$-eq for the 2°C pathway (Roelfsema et al., 2020).

In response, geoengineering is being discussed as an option to partially offset anthropogenic climate warming in order to gain more time to reduce greenhouse gas emissions. The most common methods of geoengineering considered are Carbon Dioxide Removal (CDR) and Radiative Forcing Geoengineering (RFG). While CDR aims to remove CO_2 from the atmosphere, for example, by enhancing weathering or afforestation, RFG would alter the Earth's radiation budget at the top of the atmosphere (TOA) (Lawrence et al., 2018). Of these two, only CDR addresses the problem at its root by targeting a CO_2 reduction in the atmosphere. However, it would take decades to implement CDR methods on a large scale to be efficient and they require more resources than RFG (Lawrence et al., 2018; Russell et al., 2012; Shepherd, 2009). Many proposed CDR techniques depend on the development of technologies that are not yet invented and require several technical, social and environmental issues to be solved, such as adequate carbon storage reservoirs (i.e. where can the captured carbon be stored), carbon removal potential (i.e. how much carbon can potentially be removed), governance and monitoring mechanisms, and possible adverse effects of bioenergy crops on land and water use (Lawrence et al., 2018).

RFG has been proposed to be feasible within years and thus scientists argue that it could be useful to rapidly cool global temperatures, for example, to keep the Earth system from reaching tipping points (Lawrence et al., 2018; Shepherd, 2009). Without lowering atmospheric CO_2 concentrations, RFG would have to be deployed continuously, thus inducing continuous costs. Therefore, no definitive RFG implementation costs can currently be estimated, while CDR has no further costs once the desired reduction in atmospheric CO_2 has been achieved (Lawrence et al., 2018).

Three RFG methods applied in the atmosphere are commonly proposed and studied: Cirrus Cloud Thinning (CCT), Marine Sky Brightening (MSB) and Stratospheric Aerosol Injection (SAI). All three techniques have been shown by models to have the cooling potential to limit global warming below 2°C (Lawrence et al., 2018; Lee et al., 2021). CCT aims to increase the outgoing longwave radiation at TOA by thinning high cirrus clouds that reflect longwave radiation back to Earth (Mitchell and Finnegan, 2009). MSB and SAI both act on the shortwave radiation budget of the system. In detail, MSB is designed to increase cloud coverage and reflection of sunlight over oceans (Ahlm et al., 2017; Latham, 1990) and SAI aims to build a layer of aerosols in the stratosphere that scatters part of the incoming solar radiation back to space, increasing the Earth's planetary albedo, comparable to a volcanic eruption (Kellogg and Schneider, 1974). All three RFG methods would require a long-term, continuous application to keep the global cooling intact (Lawrence et al., 2018). Upon sudden termination, RFG simulations show a rapid increase in global mean temperature - the so-called termination-shock - returning the climate system to the same warming that would have occurred without RFG (Jones et al., 2013; Lee et al., 2021). Trisos et al. (2018) simulated temperature increase rates that are two to four times higher than historical and predicted future rates for biodiversity hotspots, increasing local extinction risks as species cannot adapt or move to suitable climates in time. Hence, after applying RFG for several decades, termination can only be considered after atmospheric CO_2 concentrations have been reduced through mitigation and/or CDR to not risk a termination-shock of the climate system (Lawrence et al., 2018).

Other ideas of RFG include space-based approaches like space-mirrors or shades and surface-based methods altering the albedo of the surface. Several such schemes are proposed, such as:

- Crop albedo enhancement where crop varieties would be chosen to maximize solar reflectivity (Ridgwell et al., 2009);
- Urban albedo enhancement by using reflective materials on both roofs and pavement

(Akbari et al., 2009);

- Desert albedo geoengineering by covering not inhabited parts of deserts with reflective materials (Vaughan and Lenton, 2011).

While space mirrors would require a drastic reduction in material transport costs and have serious, insufficiently understood risks such as technical failures or asteroid impacts, surface-based approaches have been shown to either be too limited in their cooling potential or are associated with considerable side effects like the disruption of ecosystems (Lawrence et al., 2018).

While some CDR technologies have advanced to the testing phase (e.g. ocean fertilization (Yoon et al., 2018)) and some are already in operation (e.g. direct air capture plants in Iceland (climeworks, 2021)), RFG is currently still mostly untested in the field. One of the main reasons brought up by Schäfer et al. (2013) is the lack in international governance over the application of RFG. RFG would affect the global climate system and hence requires a strong international governance and supervision outside the scientific community. Further, premature application has considerable risks as there are many poorly understood effects of RFG such as overseeding clouds that could lead to warming instead of cooling (Storelvmo et al., 2013). There have been proposals for field experiments, for example, the Stratospheric Particle Injection for Climate Engineering (SPICE) and Stratospheric Controlled Perturbation Experiment (SCoPEx) projects (Morrow, 2020). Both projects were cancelled after facing public opposition due to the public not being involved enough and the fear of normalisation of such technology (Fountain, 2021; Morrow, 2020). Hence, RFG remains untested in the field up to now.

Correspondingly, Earth System Models (ESMs) are being and have been used to assess the impacts of large-scale RFG on various aspects of the Earth system to better understand the feedbacks and consequences of RFG application without employing it in the field. Some examples of previous studies comparing the atmospheric RFG methods, CCT, MSB, and SAI, have found that

- All three methods show similar global mean temperature evolutions (Muri et al., 2018);
- All three methods lead to changes in regional precipitation rates (Crook et al., 2015);
- SAI and MSB are not effective during polar nights and hence showed a reduction in cold extremes in high-latitudes (Aswathy et al., 2015).

However, there is still a lack of in-depth comparative analyses of RFG methods, as emphasised by Muri et al. (2018). In the study presented in this thesis, we use the Norwegian Earth System Model (NorESM1-ME) (Bentsen et al., 2013; Tjiputra et al., 2013) to analyse the responses and feedbacks of terrestrial systems. We use the three most commonly discussed RFG methods:

- CCT by increasing the fall speed of ice crystals for temperatures below -38°C;
- MSB by increasing the natural emission of sea salt aerosols in the accumulation mode into the atmosphere between the latitudes of 45°S and 45°N;
- SAI by prescribing the properties of an injected layer of sulfur in the stratosphere.

While numerous independent studies have confirmed the efficacy of RFG in limiting future global warming, e.g. keeping global mean temperature increase below 2°C (MacMartin et al., 2018), others have found undesirable effects on climatic conditions and related ecosystem effects under RFG implementation, such as

- Changes in precipitation patterns with a global decrease in precipitation (Keller et al., 2014);
- Significantly decreased monsoon precipitation in Western Africa (Da-Allada et al., 2020);
- Decreased ocean productivity, especially under SAI and MSB (Lauvset et al., 2017);
- Enhanced ocean acidification under SAI (Tjiputra et al., 2016);
- Dryland expansion under MSB (Park et al., 2019).

There have been some studies that have focused on the responses of Arctic ecosystems under SAI: Berdahl et al. (2014) concluded that even when reducing TOA net radiation to 2020 values, there still will be major Arctic sea ice loss, while Lee et al. (2019) found that permafrost degradation is slowed under SAI as compared to RCP8.5 but that degradation still sets in up to 40 years earlier than under RCP4.5, especially in eastern Siberia. However, there is still a lack of thorough analyses on how different RFG will impact high-latitude ecosystems. Polar regions have not been the center of attention in the RFG studies due to the short season of impact. We emphasize the importance of polar regions not only due to the amplified climate change they are undergoing, but also due to their

climatic and ecological teleconnections to mid-latitudes (Kim et al., 2022, 2017) which are fundamental in controlling the Earth's climate (IPCC, 2022). Anomalous warm periods in the Arctic can, for example, cause a cooling over North America, leading to reduced crop yield (Kim et al., 2017). It is crucial to understand the potential side effects of RFG on the Arctic and how RFG might alter the Arctic climate and ecosystems as the Arctic climate influences regions beyond the northern polar region.

RFG would cool the Earth by offsetting the radiative forcing and the greenhouse effect of CO_2, but it does not directly downregulate the high CO_2 concentration in the atmosphere (Muri et al., 2014). In addition to its greenhouse warming effect, CO_2 also indirectly influences the climate through vegetation feedbacks, with the two main processes, CO_2 fertilization and plant physiological forcing, entailing opposing effects on transpiration[4] (Park et al., 2020). While CO_2 increases the carbon uptake and leaf area index (LAI) of the plants, plant physiological forcing describes the process of plants closing their stomata under elevated CO_2 concentration to reduce water loss, hence reducing transpiration (Drake et al., 1997). Reduced transpiration in turn leads to an increased Bowen ratio of sensible heat[5] to latent heat[6], subsequently increasing the temperature of the boundary layer - the lowest part of the troposphere that is directly influenced by the Earth's surface (Ainsworth and Long, 2005; Drake et al., 1997; Lammertsma et al., 2011). The CO_2 fertilization effect was found to be dominant over changes in temperature, precipitation, and radiation for tropical forests in RFG simulations in Muri et al. (2015), generally increasing transpiration of the plants. Park et al. (2020), however, found in their simulations on plant physiological forcing that in mid- and high-latitudes the process of closing stomata outweighs the effect of increase in LAI, leading to a net decrease in transpiration. This effect can remotely influence Arctic temperatures, introducing additional positive feedback and contributing to Arctic amplification. In turn, this can lead to changes in extreme temperatures and events such as heatwaves, wildfire frequency, or permafrost thawing (Park et al., 2020). As the RFG scenarios do not directly and significantly alter the terrestrial and oceanic carbon sinks (Muri et al., 2014), they simulate a very similar atmospheric CO_2 increase as RCP8.5, subsequently increasing the effect of plant physiological forcing in the future (Lee et al., 2021). The interplay between the potential application of RFG and intensifying plant physiological forcing under unabated anthropogenic CO_2 emissions

[4]Transpiration is defined as the loss of water from a plant through its stomata (Park and Allaby, 2007).
[5]Sensible heat describes the heat that causes a change in temperature, in this case the air in the lower atmosphere (Park and Allaby, 2007).
[6]Latent heat is defined as the heat energy transferred when water changes its state (Park and Allaby, 2007).

in the future is poorly understood and represents a key knowledge gap in RFG research. It is crucial to understand how RFG impacts CO_2 related processes that are not controlled by geoengineering management, especially in a region like the Arctic that is not only heavily impacted by plant physiological forcing through heat transport (Park et al., 2020) but has also been shown to be one of the most impacted regions by global warming (IPCC, 2022).

The main aim of this thesis is to evaluate how RFG affects the extreme temperature conditions in the Arctic and its interaction with plant physiological forcing based on the existing fully interactive Norwegian Earth System Model (NorESM1-ME) simulations (e.g. Fan et al. (2021); Muri et al. (2018); Tjiputra et al. (2016)). The second aim is to evaluate the effects of changes in extreme temperature conditions on climatic conditions and their potential effects on wildfire frequency and permafrost thaw. The three RFG methods are implemented in the model such that they reduce the radiative forcing of the representative concentration pathway with 8.5 $\mathrm{W\,m^{-2}}$ radiative forcing (RCP8.5 or high-emission scenario) to 4.5 $\mathrm{W\,m^{-2}}$ (corresponding to the RCP4.5 or intermediate emission scenario) by 2100. To analyse extreme events, we assess boreal summer (JJA) maximum temperature (T_{Xx}), boreal winter (DJF) minimum temperature (T_{Nn}) and mean temperature (T_{mean}). Surface warming due to physiological forcing was found to be the highest over mid- to high-latitudes (Park et al., 2020), with the excessive surface heat energy being transported to the Arctic region, which is why we analysed not only the areas $> 65°$N but also $> 50°$N. To investigate the impact of plant physiological forcing on temperature extremes in the Arctic, we analyse the regional energy budgets and evaluate potential shifts in the flux partitioning. Lastly, we connect the RFG-induced changes in climatic conditions to Arctic terrestrial system dynamics such as fire frequency and permafrost thawing.

This thesis is structured as follows: The model, the RFG methods, and the analysis are described in section 2 (Methods). Section 3 describes the results found in this study, including the impact of RFG on Arctic extreme temperature, the effect of physiological forcing under RFG and how this impacts the Arctic terrestrial system with a focus on fires and permafrost thawing. In section 4, the results are discussed, and conclusions are drawn.

2 Methods

This section provides information and background on the methods and experimental design of the analysis of this thesis. The NorESM1 model is described in section 2.1, followed by a description of the three RFG methods, CCT, MSB, and SAI, in section 2.2 and the analysis of the model output in section 2.3. Section 2.4 describes the experimental design and section 2.5 explains how the linear regression analysis was set up.

2.1 Model description

To assess the influence of RFG on the Arctic terrestrial system, we used the model output of the fully coupled Norwegian Earth System Model (NorESM1-ME) described in detail by Bentsen et al. (2013), and Tjiputra et al. (2013). NorESM1-ME is based on the Community Climate System Model version 4 (CCSM4) and contains prognostic biogeochemical cycling. Changes from CCSM4 relevant for this analysis are a modified chemistry-aerosol-cloud-radiation scheme (Kirkevåg et al., 2013) and coupling of the ocean carbon cycle model with an isopycnic ocean general circulation model (Tjiputra et al., 2013). The model participated in phase 5 of the Climate Model Intercomparison Project (CMIP5), and the Geoengineering Model Intercomparison Project (GeoMIP). It has a resolution of 1.9° latitude by 2.5° longitude and 26 vertical layers (Bentsen et al., 2013). The model output variables used in this analysis are summarised in Table 1.

2.2 Radiative forcing geoengineering methods

The model outputs analysed here simulate the implementation of three RFG methods: Cirrus cloud thinning (CCT), marine sky brightening (MSB), and stratospheric aerosol injection (SAI). They are designed such that they reduce the radiative fluxes at the top of the atmosphere from the RCP8.5 levels to that of the RCP4.5 scenario, requiring a radiative forcing of -4 Wm^{-2} by 2100. Geoengineering is applied for 81 years, starting in 2020. For each RFG method three different simulation ensembles are run with small perturbations to the initial conditions in the year 2020 to simulate uncertainties in the model (Muri et al., 2018). For the baseline scenario, one simulation for the RCP8.5 scenario was carried out, running from 2006-2100.

CCT aims to thin out high ice clouds, i.e. cirrus, that act to trap longwave radiation in the climate system through absorption and re-radiation of terrestrial radiation and thus

Table 1: Description of the analysed NorESM1 output variables.

Name	Long Name	Model
TS	Surface temperature (radiative) [K]	Atmospheric
TREFMXAV	Daily maximum of average 2-m temperature [K]	Land surface
TREFMNAV	Daily minimum of average 2-m temperature [K]	Land surface
FCTR	Canopy transpiration [W/m^2]	Land surface
LHFLX	Surface latent heat flux [W/m^2]	Atmospheric
SHFLX	Surface sensible heat flux [W/m^2]	Atmospheric
FSNSC	Clearsky net solar flux at surface [W/m^2]	Atmospheric
FSNS	Net solar flux at surface [W/m^2]	Atmospheric
FSDS	Downwelling solar flux at surface [W/m^2]	Atmospheric
FLNSC	Clearsky net longwave flux at surface [W/m^2]	Atmospheric
FLNS	Net longwave flux at surface [W/m^2]	Atmospheric
RAIN	Atmospheric rain [mm/s]	Land surface

have a net warming effect on the Earth system (Lawrence et al., 2018). By thinning these clouds, more longwave radiation can escape to space, altering the Earth's radiation budget. This can be achieved by seeding ice nuclei in regions where cirrus clouds form to initiate heterogeneous freezing and the formation of larger crystals that may fall out of the clouds, thereby thinning them out (Mitchell and Finnegan, 2009). At temperatures colder than -40°C homogeneous freezing is favoured if the supersaturation is higher than 50% with respect to ice. Since heterogeneous freezing requires a lower supersaturation, it will be favoured if the ice nuclei concentration is high enough (Muri et al., 2014). By increasing the number of cloud condensation nuclei (CCN), heterogeneous freezing can dominate and deplete the clouds of water vapor. Mitchell and Finnegan (2009) suggested Bismuth triiodide (BiI_3) as a potential seeding material as it is relatively cheap and non-toxic, and Lawrence et al. (2018) proposed that the seeding material could be injected at the required troposphere level via aircraft or drones. In NorESM1, the method was implemented as follows (Muri et al., 2014): As an analogy to cloud seeding, CCT is approximated by increasing the fall speed of crystals for temperatures colder than -38°C, the temperature where typically homogeneous freezing sets in. The fall speed was increased by a factor of up to ten by the end of the century. This simulation experiment is an oversimplification

as physical processes such as the injection of ice nuclei into the upper troposphere or the growth into ice crystals are not simulated.

MSB acts on the shortwave energy budget of the Earth system by enhancing the concentration of droplets in low marine stratocumulus clouds, increasing the cloud albedo. The suggested method is to inject ocean water mist into the lower atmosphere in regions where there is a deficit of CCN. The sodium chloride (NaCl) remaining from the evaporating water would hereby function as CCN (Latham, 1990, 2002). Due to the lack of CCN, the number of droplets in marine clouds are approximately one order of magnitude smaller than over land (Latham, 1990). Latham et al. (2008) highlighted the potential of MSB by estimating that a 6% increase of the albedo of marine stratocumulus clouds could offset the warming of an atmospheric CO_2 doubling. The increase in albedo is not the only mechanism causing the cooling, as the direct effect of the bright sea salt aerosols is also contributing to the cooling in the model, as established in Mitchell and Finnegan (2009). MSB differs from the other two RFG methods as the reduction in solar radiation is almost exclusively happening over the ocean regions, rather than both over land and ocean (Bala et al., 2011), leading to a more heterogeneous cooling (Lawrence et al., 2018). Injection could be performed by autonomous ships, releasing micron-sized drops of seawater into the boundary layer below marine stratocumulus clouds (Salter et al., 2008). MSB is implemented in NorESM1 following the method of Alterskjær and Kristjánsson (2013) by increasing the natural emission of sea salt aerosols in the accumulation mode from the ocean surface to the lower atmosphere between the latitudes of 45°S and 45°N. To achieve the required -4 Wm^{-2} in radiative forcing, the ocean area where CCN are emitted was increased as compared to Alterskjær and Kristjánsson (2013) who limited their area to the latitudes between 30°S and 30°N. By the end of the century, emissions of 460 Tg yr^{-1} of sea salt were required over the whole area (Muri et al., 2018).

Similar to MSB, SAI affects the shortwave radiation budget of the Earth. SAI is the most studied RFG approach as it is based on the natural dimming following volcanic eruptions. In this approach, aerosols like sulfur dioxide (SO_2) are injected into the stratosphere, building a layer of aerosols that effectively scatter part of the incoming solar radiation, increasing the Earth's planetary albedo (Crutzen, 2006; Kellogg and Schneider, 1974). The best global distribution can be achieved through aerosol injection in the tropics as the Brewer-Dobson circulation leads to an effective dispersion towards the poles (Jones et al., 2017) but leaves little control over regional distributions (Lawrence et al., 2018). Stratospheric aerosols have a residence time of 1-3 years, dictating the frequency with which SAI has to be applied (Benduhn and Lawrence, 2013; Niemeier et al., 2011).

Proposed injection techniques include aircrafts, pipes suspended by floating platforms, rockets, and stratospheric balloons (Davidson et al., 2012; McClellan et al., 2012), all of which require further research and technological development (Lawrence et al., 2018). The implementation of SAI in NorESM1 is modelled according to the description of Tilmes et al. (2015): SO_2 is injected into the stratosphere at a grid point close to the equator at a height of around 20 km (60 hPa). The following distribution of the SO_2 was simulated using an interactive aerosol microphysics module (HAM) of the general circulation model ECHAM5. Muri et al. (2018) found that the needed emission strength to offset 4 Wm^{-2} radiative forcing requires 5 Tg(S) yr^{-1} in 2050, increasing to 10 Tg(S) yr^{-1} in 2075 and 20 Tg(S) yr^{-1} in 2100.

2.3 Analysis of model output

The relevant output variables were extracted with a Linux PowerShell (see Appendix 7.1) that extracts the full time series of each indicated variable for each ensemble as a single file. The files were analysed in Python 3.9.7. The codes used to generate the results and figures of this work are available at the GitHub repository (https://GitHub.com/RhondaMueller/Codes-RFG-Arctic-Impacts.git).

2.4 Experimental design

Our aim is to compare the RFG methods to the RCP8.5 simulation at the same level of global mean temperature increase of 2°C as we expect large differences in temperature extremes between RFG and RCP8.5, even though the global mean temperature increase is the same. 2°C was chosen as it is the aimed for maximum temperature increase of the Paris Agreement. As was shown by Seneviratne et al. (2016), the global mean temperature increases linearly with CO_2 emissions but due to plant physiological forcing, temperature extremes in the Arctic might behave differently under RFG. Since under RFG the global mean temperature increase of 2°C is achieved later than under RCP8.5, CO_2 will be higher by then. Hence, we expect to see large differences in temperature extremes in the Arctic due to plant physiological forcing. We determined for every ensemble, the year it reaches the 2°C global mean temperature increase (289.15°K) compared to the pre-industrial mean. We calculated the pre-industrial mean from NorESM1 simulations as the mean of global temperatures from a 500-year control simulation. The data were handled as a 21-year running mean to be able to analyse long-term trends. The centred

year here refers to the median year of the 21-year time period (e.g. the centred year of the 2030-2050 running mean is 2040). We calculated anomalies with respect to the mean of the first 21 years of the RCP8.5 scenario (2006-2026). This time frame was chosen to simplify the analysis, as it was easily available for all variables used in this analysis. Further, our analysis is not sensitive on the time frame of the baseline scenario. As we are interested in the land processes in the Arctic, most variables were considered only over land. The only exception is the global mean temperature that was considered over land and ocean (T_{glob}). To calculate the mean over an area, the value of each grid cell within the area is weighted with the cosine of its latitude. The three ensembles of each RFG were generally taken as a mean for each RFG method. The maximum temperature (T_{Xx}) was calculated as the maximum temperature of the JJA months for each year, minimum temperature (T_{Nn}) as the minimum temperature of the DJF months for each year (December being taken from the year before) and mean temperature (T_{mean}) as the mean temperature of all months of the respective year. We defined albedo as the ratio of upward over downward shortwave radiation at the surface. The Bowen ratio was calculated as the ratio of sensible heat over latent heat and the corresponding uncertainty as the square root of the quadratic sum of the relative uncertainties for sensible and latent heat.

Previous studies show that fire frequency increases under hot and dry conditions (Jain et al., 2022; Jolly et al., 2015; Kharuk et al., 2021; Young et al., 2017), and Arctic fires are particularly sensitive to boreal summer temperatures (Kharuk et al., 2021; Young et al., 2017). To assess how the Arctic temperature conditions under RFG might affect fire frequency, we analysed current climatic conditions of fire occurrence during boreal summer between 2001 and 2020 for a satellite data-driven fire frequency dataset (MCD64). We further analysed the T_{Xx} and T_{mean} conditions under RCP8.5 where RCP8.5 reaches 2°C global warming (centred year 2040) by counting occurrences of given T_{mean} and T_{Xx} anomalies in the region north of 50° N (Figure 7b) and how temperature conditions shift under CCT and MSB (Figure 7c, d). The temperatures for fire conditions were analysed for the region north of 50°N instead of 65°N to include the boreal forest and its boundary to the tundra, both regions that were found to be vulnerable to climatically induced changes in fire activity (Young et al., 2017). We determined the temperature conditions by analysing bins of the size 0.6 by 0.6°C and evaluating how often each T_{Xx} and T_{mean} combination is present in all the land grid cells north of 50°N, divided by the number of total land grid cells north of 50°N. Only grid cells that contain at least 50% of boreal plant function types (needleleaf evergreen boreal tree, needleleaf deciduous boreal tree,

broadleaf deciduous boreal tree, broadleaf deciduous boreal shrub, and arctic grass) were considered. Each bin thus contains the probability of each T_{Xx}, T_{mean} combination, which is further referred to as frequency. We calculated the fire frequency in a similar way by calculating the burned area for the respective temperature conditions from the MCD64 monthly burned area dataset from 2001 to 2020 and the same time frame for the temperature anomalies (Giglio et al., 2015). As single heat events are important for fires, we considered the JJA months separately. To determine anomalies, T_{Xx} and T_{mean} were calculated for each grid cell for the RCP8.5 2006-2026 period and subtracted from T_{Xx} and T_{mean} of that grid cell when the scenarios reach the 2°C global mean temperature increase.

Similar to fires that release CO_2 by burning organic matter, permafrost thawing may accelerate global scale warming by releasing large amounts of organic matter storage (Schuur et al., 2008) as greenhouse gas emissions (Schuur et al., 2015). We hypothesise that permafrost may continue to thaw faster with the strong increase of the minimum temperatures over several years. We focus on SAI to test this hypothesis as SAI is the only scenario where boreal winter minimum temperatures north of 65°N differ from the other scenarios. To assess how the Arctic temperature conditions under RFG might affect the permafrost fraction, we analysed current climatic conditions of permafrost areas during boreal winter between 2003 and 2019. The permafrost fraction, defined as the percentage of the grid cell underlain by permafrost, was taken from the dataset of the European Space Agency's Climate Change Initiative Permafrost project and covers the period from 2003 to 2019 (Obu et al., 2021). We further analysed the T_{Nn} and T_{mean} conditions under RCP8.5 where RCP8.5 reaches 2°C global warming (centred year 2040) by counting occurrences of given T_{mean} and T_{Nn} anomalies in the Arctic (Figure 8b) and how temperature conditions shift under SAI (Figure 8c). We determined the temperature conditions by analysing bins of the size 2.0 by 3.0°C and evaluating how often each T_{Nn} and T_{mean} combination is present in all the land grid cells north of 65°N, divided by the number of total land grid cells north of 65°N. Each bin thus contains the probability of each T_{Nn}, T_{mean} combination. The DJF months were taken as mean, since longer cold or warm periods are more influential than short events for the permafrost fraction. No anomalies were determined for T_{Nn} as permafrost thawing depends on absolute temperatures and is not anomaly-driven like fires.

2.5 Linear regression analysis

To assess the spatial differences between the RFG and the RCP8.5 scenarios we performed a linear regression (LR) analysis. We calculated the T_{glob} temperature series of each ensemble for the timespan 2006-2100 for RCP8.5 and 2020-2100 for RFG with a cosine weighted mean and a 21-year running mean. In the example of Figure 5a, we calculated the JJA mean of transpiration as 21-year running mean for every land grid cell for all three CCT ensembles and the RCP8.5 scenario and evaluate its dependence on T_{glob} using linear regression. We performed a LR for every land grid cell with T_{glob} as independent and the transpiration of that grid cell as dependent variable for every ensemble. The difference in slope plotted in Figure 5a represents the difference of the mean LR slope of the three CCT ensembles and the RCP8.5 slope.

To test for significance of the differences between CCT and RCP8.5 we calculated the residual of the CCT temperature values once with the results of the LR of RCP8.5 and once with the results of the LR of CCT for each grid cell and compare those residuals with an unpaired t-test. Assuming there are no differences between CCT and RCP8.5, equation (1) should yield the same result for the LR results for both CCT and RCP8.5:

$$b = T_{Xx,CCT(n)}[i] - m_{RCPorCCT(n)} \cdot T_{mean,CCT(n)}[i] - a_{RCPorCCT(n)}, \tag{1}$$

where n = 1, 2, 3 represents the three CCT ensembles, i is for centred year of the 21-year running mean, m is the slope for RCP8.5 and the three CCT ensembles, and a the intercept for RCP8.5 and the three CCT ensembles. Hence, when conducting a t-test for the b-values obtained for the slope and intercept of the RCP8.5 LR and the b-values obtained for the slopes and intercepts of the CCT LRs, p-values <0.05 indicate that there is a significant difference between the LRs of CCT and RCP8.5.

3 Results

3.1 Mean and extreme temperature increase under RFG in the Arctic

Figure 1 shows the increase in mean temperature (T_{mean}, Figure 1a), maximum temperature (T_{Xx}, Figure 1b), and minimum temperature (T_{Nn}, Figure 1c) for the land area north of 50°N (a, b, c) and the Arctic region (north of 65°N; d, e, f) per global mean temperature (T_{glob}) increase for the three RFG and RCP8.5 time series (2020-2100 for RFG and 2006-2100 for RCP8.5).

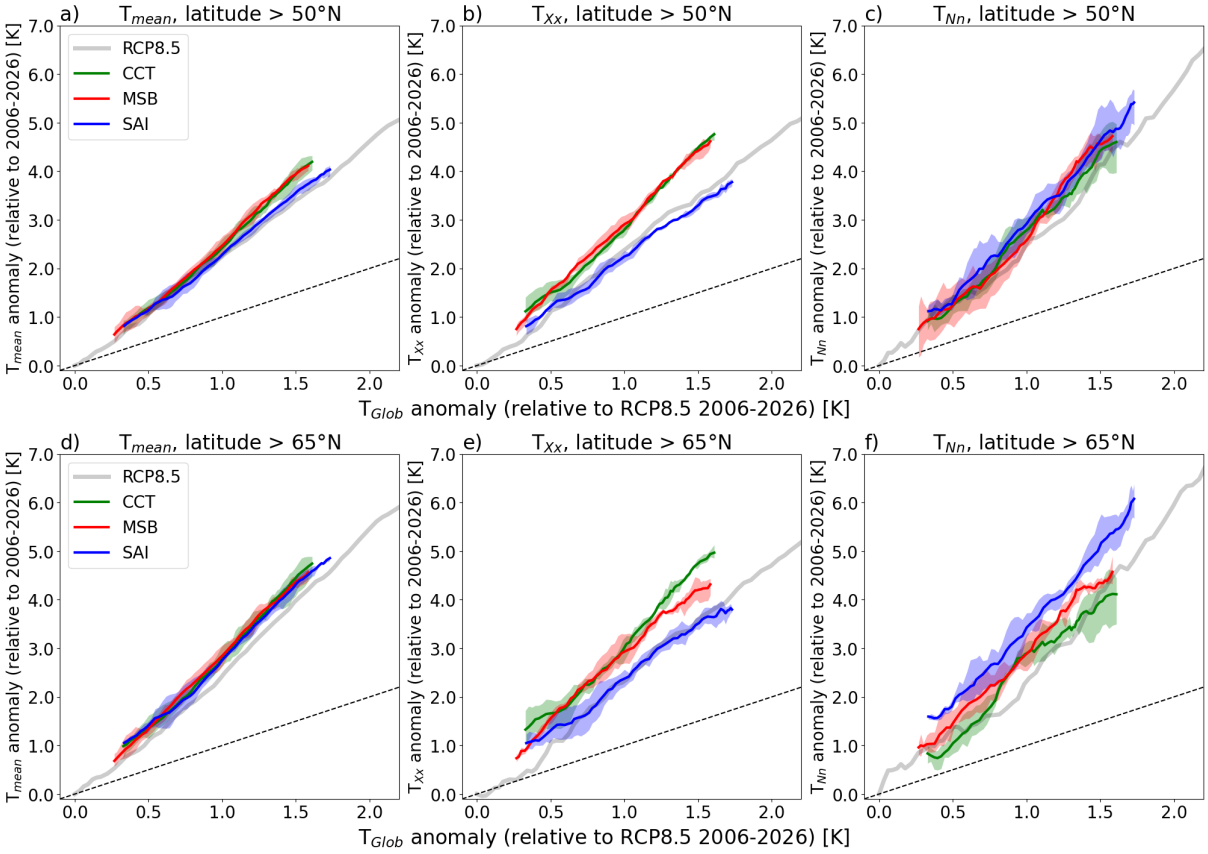

Figure 1: a,b,c) Anomaly in mean (T_{mean}), maximum (T_{Xx}) and minimum (T_{Nn}) land temperature north of 50°N compared to the global mean temperature (T_{glob}) anomaly over land and ocean. d,e,f) Anomaly in mean (T_{mean}), maximum (T_{Xx}) and minimum (T_{Nn}) land temperature north of 65°N compared to the global mean temperature anomaly over land and ocean (T_{glob}). The yearly anomalies of RCP (CCT; MSB; SAI) represented by the grey (green; red; blue) line are evaluated with respect to the mean of RCP8.5 from 2006-2026. The lines represent the ensemble mean. The ensemble spread is shaded. The hatched line represents the 1:1 line.

Our results show that all three RFG methods are not effective in reducing temperature increase in the Arctic, but closely follow or even exceed warming rates of the RCP8.5 scenario (Figure 1). Similar to the RCP8.5 scenario, they all closely follow the current Arctic amplification trend with two to three times as much warming in the Arctic as the global mean T_{glob} (Koenigk et al., 2020). Seneviratne et al. (2016) have already shown that increases in extreme temperature such as T_{Xx} and T_{Nn} in the Arctic under greenhouse warming scenarios (e.g. RCP8.5) are higher than in T_{glob}. We show that under RFG, especially CCT and MSB, the increase in T_{Xx} is even more amplified compared to RCP8.5 north of 50°N indicating stronger intensity of heatwaves (Figure 1b and Figure 2). SAI shows a similar increase in T_{Xx} with T_{glob} as RCP8.5. Contrary to T_{Xx}, the three different RFG methods do not show significant differences in T_{Nn} north of 50°N (Figure 1c) among each other nor compared to the RCP8.5 scenario.

When considering the land area north of 65°N, T_{mean} (Figure 1d) and T_{Xx} (Figure 1e) show similar projections to Figure 1a and Figure 1b. In Figure 1f, however, SAI shows a significant difference with a higher increase in T_{Nn} per °C increase in T_{glob}. This result implies that SAI is not as effective in cooling down minimum temperatures in high

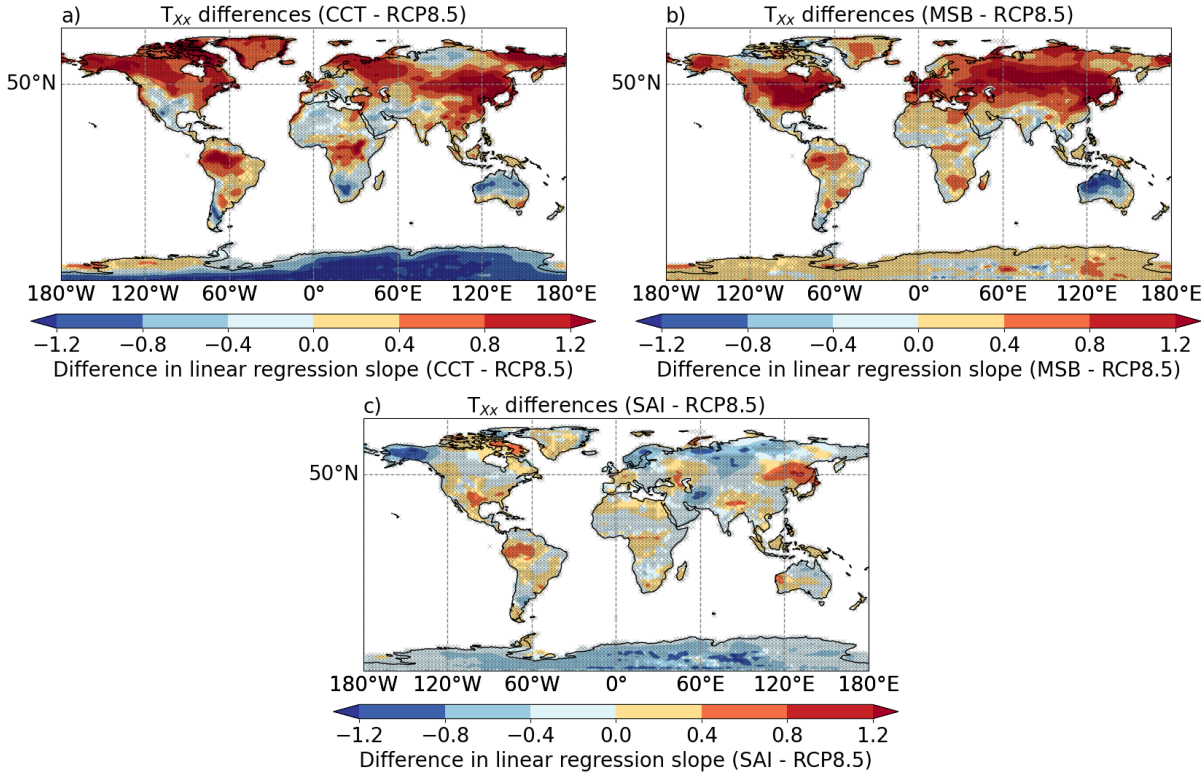

Figure 2: Global pattern of the difference between the RCP8.5 and the RFG scenarios in the slope of the linear regression between T_{Xx} of each grid cell and the T_{glob}. Areas with a significant difference in slope of RCP8.5 and RFG scenarios are hatched.

latitudes. A potential explanation could be the latitudinal temperature gradient with lower latitudes cooling more than higher latitudes under SAI especially during the polar nights due to the aerosols being injected in the equator region (Lawrence et al., 2018).

Figure 2 shows the differences of the slope of the linear regression model of T_{Xx} increase per T_{glob} increase between the three RFG methods and RCP8.5 (see section 2. Methods). In regions with a positive difference in slope, the RFG scenario will have a higher T_{Xx} than RCP8.5 for the same global mean temperature increase. Both CCT and MSB show the largest positive difference in slope in the Northern hemisphere. This indicates that under CCT and MSB, T_{Xx} increases more with T_{glob} than under RCP8.5 in mid- and high-northern latitudes (Figure 2a,b). As already shown in Figure 1, SAI has the smallest deviations from RCP8.5 in T_{Xx}, with a very similar increase of T_{Xx} with T_{glob} as RCP8.5 (Figure 2c) in the Arctic as well as over the global land area.

Similarly, when considering the spatial differences of the slope of the linear regression model of T_{Nn} per T_{glob} increase, SAI is showing different patterns than the other scenarios (Figure 3). CCT and MSB show some areas where T_{Nn} increases significantly more with T_{glob} than under RCP8.5, while in other areas T_{Nn} increases significantly less with T_{glob} as

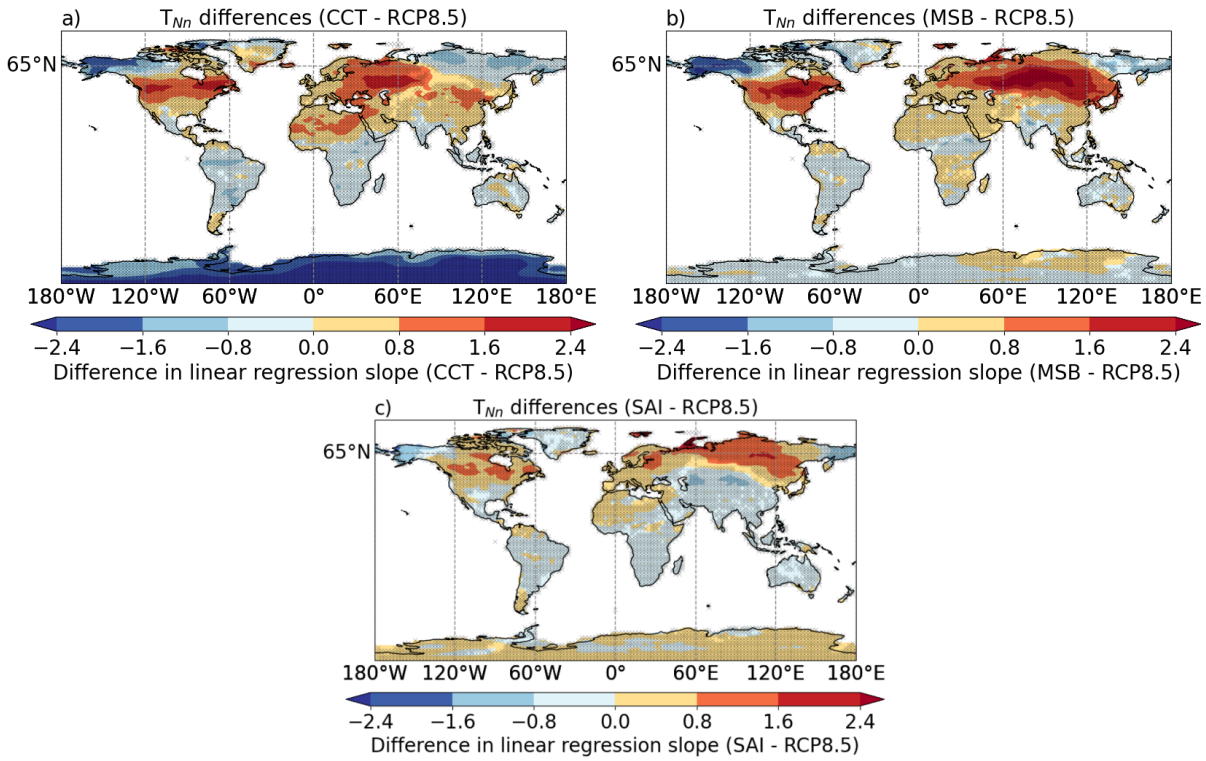

Figure 3: Global pattern of the difference between the RCP8.5 and the RFG scenarios in the slope of the linear regression between T_{Nn} of each grid cell and the T_{glob}. Areas with a significant difference in slope of RCP8.5 and RFG scenarios are hatched.

compared to RCP8.5, with the largest positive difference in slope again being seen in the Northern hemisphere (Figure 3a,b). SAI, on the other hand, shows positive differences to RCP8.5 in all areas north of 65°N except for slight negative differences in eastern Siberia and Greenland (Figure 3c).

3.2 Change in energy budget components

A possible explanation for the identified temperature anomalies under RFG might be found in plant physiological forcing. To verify this hypothesis, the energy budget components during boreal summer, when plant physiological forcing is strongest, are analysed. We expect to see changes in the energy budget as a result of plant physiological forcing due to the effect of closing plant stomata under a high CO_2 concentration environment to save water. With closing of the stomata comes a decrease in transpiration and its associated cooling effect (Skinner et al., 2018). This could explain the increase in extreme temperatures seen under RFG in the latitudes north of 50°.

We found that the transpiration amount was significantly reduced under all three RFG methods north of 50° relative to RCP8.5 at comparable global warming of 2° (Figure 4). We see in the spatial pattern of the differences in increase of transpiration per increase in T_{glob} that for all three RFG methods practically all land regions north of 50° show a negative difference in slope compared to RCP8.5 (Figure 5a, d, g). This demonstrates that all three RFG methods show less increase of transpiration with global warming in the regions north of 50° than RCP8.5. Even though the three RFG methods show different signs in the change of latent and sensible heat, we see an increased Bowen ratio compared to RCP8.5 under all three RFG methods (Figure 4 and Table 2).

While we see reduced transpiration as compared to RCP8.5 during boreal summer in the

Table 2: Sensible Heat, Latent Heat and Bowen Ratio for RCP, CCT, MSB and SAI during boreal summer at the time when each scenario reaches 2°C global warming.

	Sensible Heat [W/m^{-2}]	Latent Heat [W/m^{-2}]	Bowen Ratio
RCP	37.13±0.44	46.36±0.67	0.801±0.019
CCT	39.21±0.29	46.74±0.20	0.839±0.008
MSB	38.82±0.28	45.86±0.20	0.847±0.008
SAI	36.46±0.21	44.86±0.27	0.813±0.008

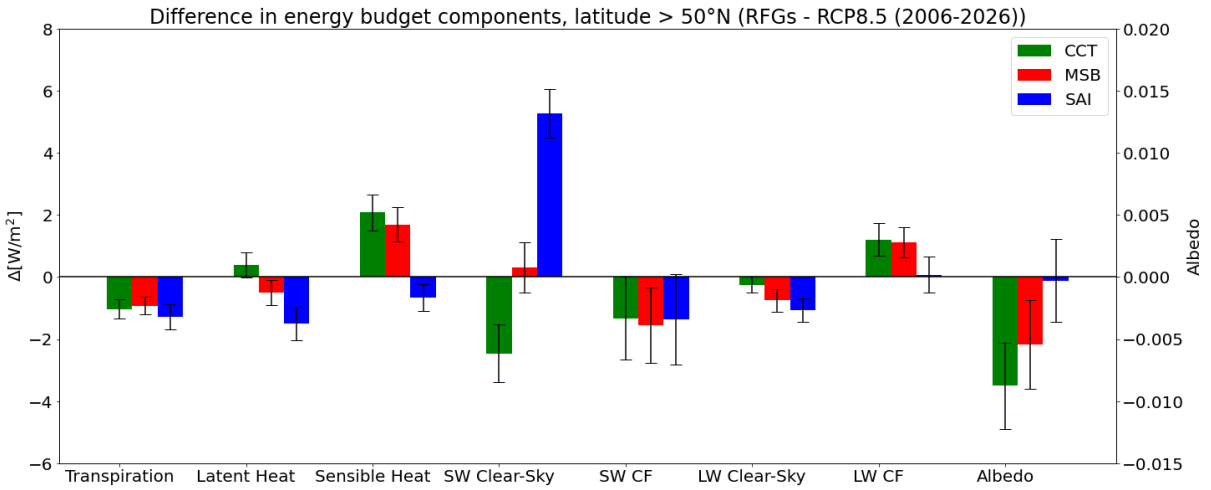

Figure 4: Difference of the energy budget components > latitude 50°N during boreal summer from the initial values from the first 21 years of the RCP8.5 scenario to when each scenario reaches the 2°C global warming as compared to the pre-industrial mean. For albedo, the right y-axis applies; for all other variables the left y-axis. The skewers indicate 95% confidence intervals. Incoming fluxes are defined as negative, outgoing fluxes as positive. SW stands for shortwave, LW for longwave, and CF for cloud forcing.

Arctic under all three RFG methods, an increase in sensible heat is only seen in CCT and MSB (Figure 4). The spatial patterns of CCT and MSB in sensible heat are very similar, both showing a significant positive difference in slope of sensible heat versus T_{glob} as compared to RCP8.5 in almost the entire region north of 50°N (Figure 5c,f). CCT has a slightly larger positive difference in slope than MSB overall, also seen in Figure 4. Of the three RFG methods, CCT is the only method that shows increased latent heat in the Arctic during the boreal summer (Figure 5b and 4) indicating a strengthened hydrological cycle (Kristjánsson et al., 2015) which is also illustrated in the precipitation pattern, where CCT shows a general increase in precipitation in the Arctic (Figure 6). While SAI does show a slight increase in Bowen ratio during boreal summer - as expected by physiological forcing - sensible heat is decreased as compared to RCP8.5. Considering the spatial pattern, we see that the negative difference in sensible heat per increase in T_{glob} between SAI and RCP8.5 is mainly in the high-latitude regions (Figure 5i). When comparing this to the pattern of T_{Xx} in Figure 2c discussed above, the areas of largest decrease for both sensible heat and T_{Xx} are Scandinavia, Alaska, and Siberia, indicating that less increase in sensible heat per increase in T_{glob} also causes less increase in T_{Xx} per increase in T_{glob}.

SAI further shows significant differences to CCT and MSB when considering the shortwave radiation in the Arctic at the time when the scenarios reach the 2°C global mean

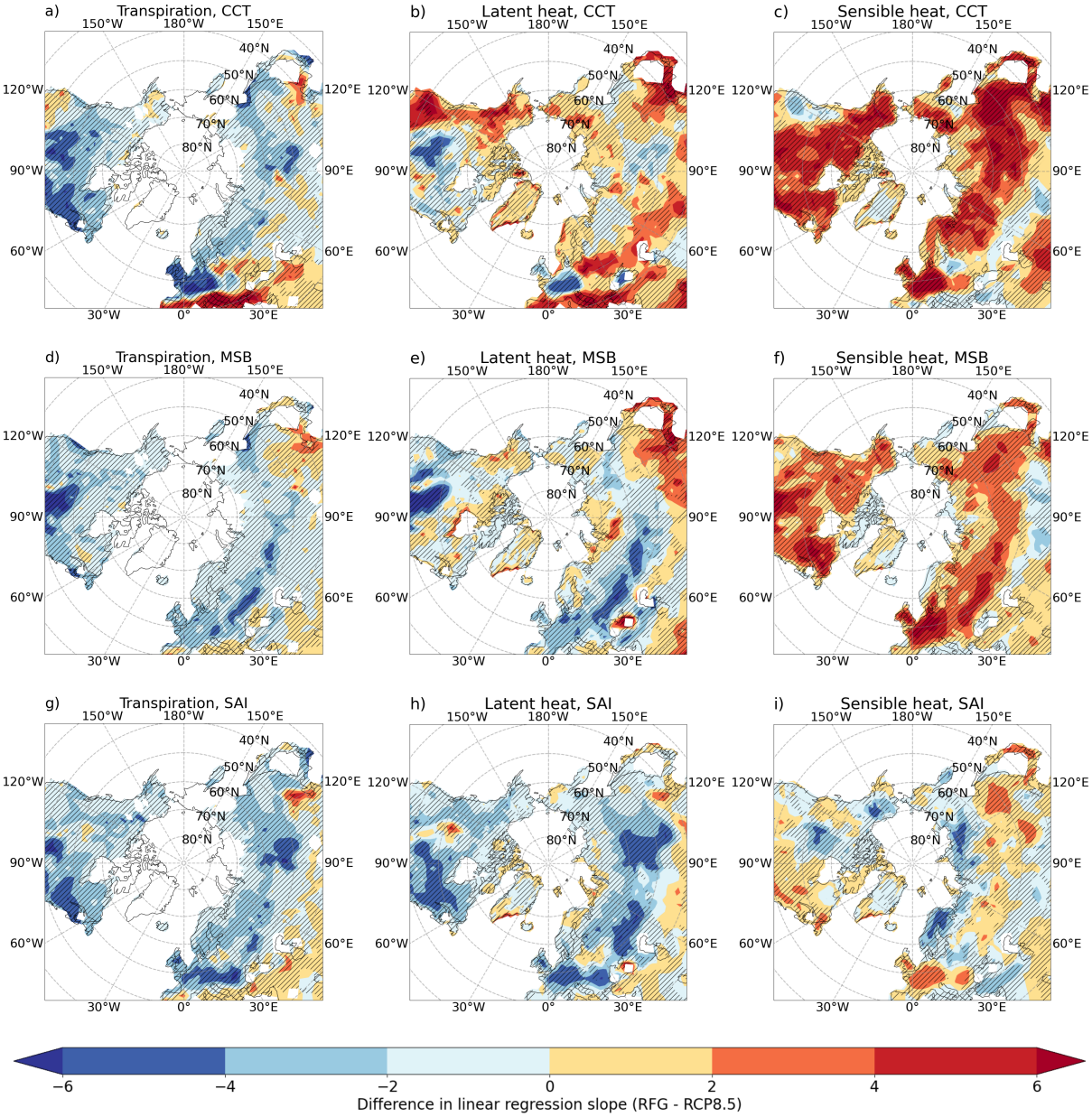

Figure 5: Simulated change of transpiration (left), latent heat (middle), and sensible heat (right) during boreal summer in the Arctic for CCT, MSB, and SAI. Pattern of the difference between the respective RFG scenarios and the RCP8.5 scenario in the linear regression slope between transpiration, latent heat, and sensible heat, respectively, and T_{glob}. Areas with a significant difference in slope of RCP8.5 and RFG scenarios are hatched.

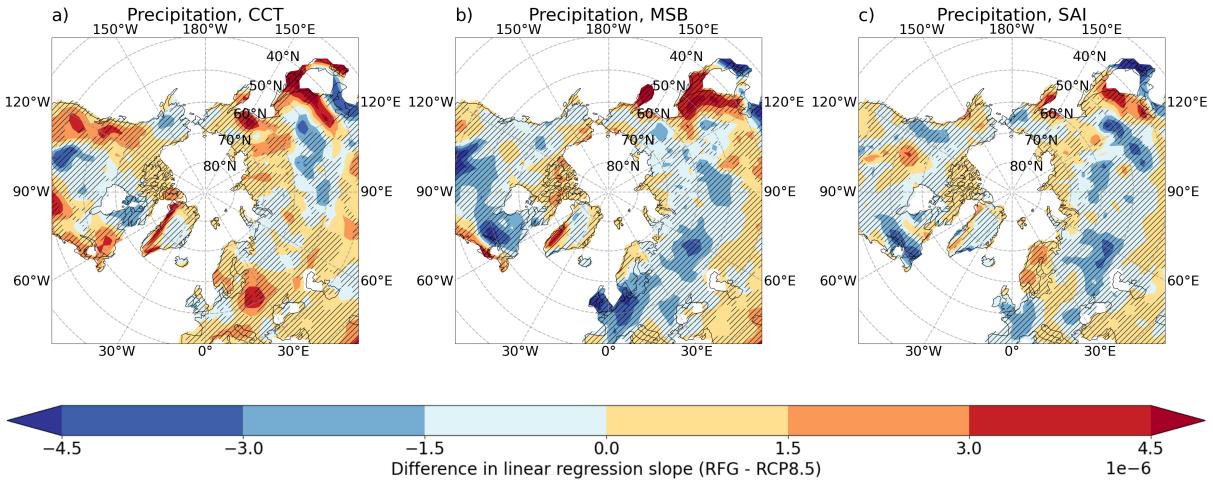

Figure 6: Pattern of the difference between the respective RFG scenarios and the RCP8.5 scenario in the linear regression slope between precipitation during boreal summer and T_{glob}. Areas with a significant difference in slope of RCP8.5 and RFG scenarios are hatched.

temperature increase as compared to the pre-industrial temperatures (Figure 4). While we found a decreased shortwave cloud forcing of similar magnitude in all three RFG scenarios, the incoming clear-sky shortwave radiation significantly differs between them. In Figure 4, we defined outgoing fluxes as positive while incoming fluxes as negative. The negative sign in incoming clear-sky shortwave radiation under CCT thus signifies a significant increase in incoming clear-sky shortwave radiation while the positive sign under SAI signifies a significant decrease in clear-sky shortwave radiation. MSB does not deviate significantly from RCP8.5. All three RFG methods show a slight decrease in clear-sky longwave radiation as compared to RCP8.5. The albedo of SAI in the Arctic during boreal summer is the closest to the one of RCP8.5, not being significantly different, while CCT and MSB both show a significant decrease in albedo.

3.3 Impacts on Arctic system dynamics

In a last step, we assess how shifts in temperature extremes found under RFG affect the projected fire frequency and permafrost thawing in the Arctic. We have already shown that under CCT and MSB, maximum summer temperature increases more with T_{glob} than under RCP8.5 and SAI, potentially leading to climatic conditions with more frequent fire activity in the Arctic. Our results show that during the period of 2001-2020 the majority of fire events occur when T_{Xx} anomalies are higher than T_{mean} anomalies during the months of June, July, and August (Figure 7a), indicating that T_{Xx} is a stronger driver

for fire frequency than T_{mean} and that larger increases in T_{Xx} than T_{mean} could increase fire activity in high-latitudes. The simulated temperature frequency distribution when RCP8.5 reaches 2°C global warming shows that the most common temperature conditions

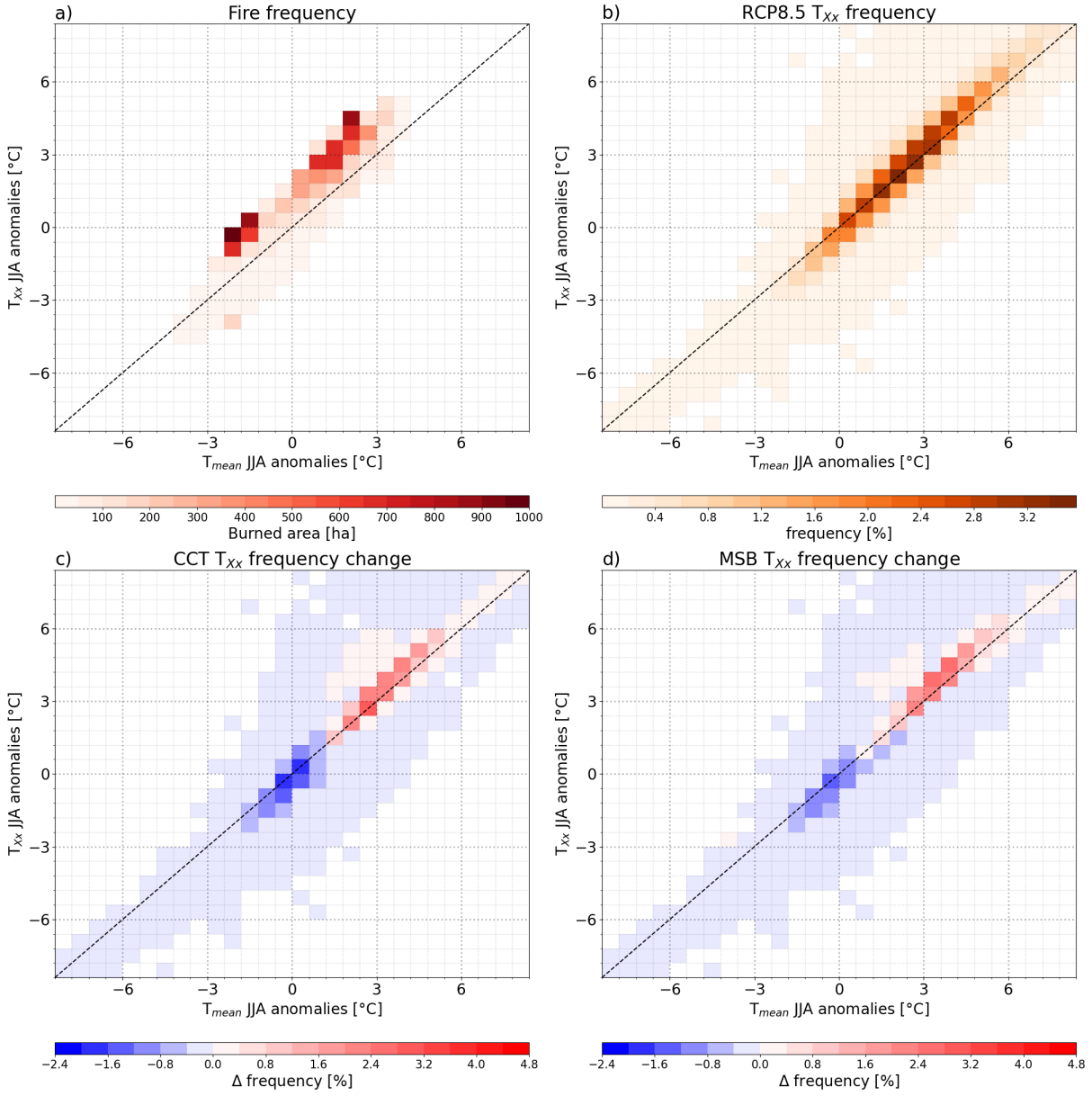

Figure 7: Change in JJA maximum temperature frequency in CCT and MSB related to fire frequency north of 50°N. a) conditions under which fires are currently observed in the Arctic (Giglio et al., 2015). The anomalies are calculated with respect to 2001-2020. b) maximum temperature frequency north of 50°N when the RCP8.5 scenario reaches 2°C global mean temperature increase as compared to pre-industrial. c-d) difference of the maximum temperature frequency between when CCT and MSB reach the 2°C global mean temperature increase and when the RCP8.5 scenario reaches 2°C increase. The hatched line represents the 1:1 line.

show similar T_{Xx} and T_{mean} anomalies (Figure 7b). However, under CCT and MSB, these conditions shift towards T_{mean} anomalies combined with higher T_{Xx} anomalies, particularly for T_{mean} anomalies around 3°C (Figure 7c, d). These are favourable climatic conditions for fire activity as we have shown in Figure 7a. This result suggests that temperature conditions under CCT and MSB shift towards conditions where fire frequency is higher than under RCP8.5 for the 2°C global mean temperature increase.

The current distribution of permafrost fraction against temperature conditions (T_{mean} versus T_{Nn}) shows that the permafrost fraction is highest below -10°C T_{mean} and is more sensitive to T_{Nn} for mid T_{mean} ranges where small changes in T_{Nn} or T_{mean} can cause large changes in permafrost fraction (Figure 8a). The T_{Nn}, T_{mean} frequency distribution of RCP8.5 when the scenario reaches 2°C global warming shows that the most common temperature conditions are around -15°C T_{mean} and -30°C T_{Nn} (Figure 8b). We noticed that under SAI the region of the highest frequency of T_{Nn} and T_{mean} conditions shifts towards higher T_{Nn}, where temperature conditions are less favourable for permafrost to occur (Figure 8c). The maximum differences in frequency are around -10°C T_{mean}, where the permafrost fraction might be particularly sensitive to changes in temperature. We found that 29 grid cells north of 65° change from T_{Nn} below 0° in 2006-2026 to above 0° in 2080-2100 in the SAI scenario. This corresponds to 3.9% of the land area north of 65°N

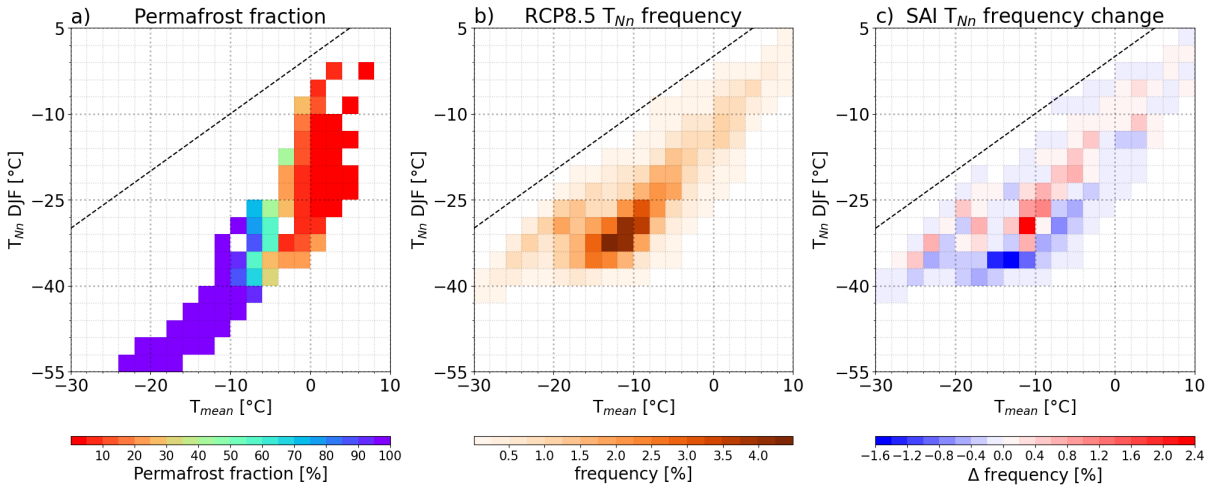

Figure 8: Change in DJF minimum temperature frequency in SAI related to permafrost north of 65°N. a) conditions under which permafrost is currently observed in the Arctic (Obu et al., 2021). b) minimum temperature frequency north of 65°N when the RCP8.5 scenario reaches 2°C global mean temperature increase as compared to pre-industrial. c) difference of the minimum temperature frequency between when SAI reaches the 2°C global mean temperature increase and when the RCP8.5 scenario reaches 2°C increase. The hatched line represents the 1:1 line.

or 628 879 km^2. 7.2% of the area changes from T_{mean} below 0° in 2006-2026 to above 0° in 2080-2100. Our results indicate that under SAI, the climatic conditions in the Arctic will be less favourable for permafrost when compared to RCP8.5 when the two scenarios reach the 2° global mean temperature increase.

4 Discussion and Conclusions

We have shown that all three of the RFG methods evaluated fail to significantly reduce mean and extreme temperature increase compared to the RCP8.5 scenario, and even worse, might introduce additional risks to the Arctic terrestrial system at a 2°C global climate warming level. Further, it has to be emphasised that RFG is implemented to reduce the global temperature increase from RCP8.5 to RCP4.5 - hence when comparing RFG to RCP4.5 we would expect even more extreme differences in the Arctic region. The changes observed in the energy budget components in CCT and MSB support the hypothesis that the larger increase of T_{Xx} with T_{glob} seen under both CCT and MSB north of 50°N can be explained by increased plant physiological forcing. The increase in sensible heat seen under CCT and MSB agrees with the found increase in boundary layer temperatures (Miralles et al., 2014; Seneviratne et al., 2010) and can lead to an increased heatwave frequency (Kala et al., 2016; Skinner et al., 2018). At 2°C warming, SAI does not deviate significantly from RCP8.5 in T_{Xx}. While the decrease in transpiration and increased Bowen ratio indicate enhanced plant physiological forcing for all three RFG methods, the effect in SAI is potentially offset due to changes in shortwave radiation, leading to higher surface albedo as compared to the other RFG methods. The differences seen in T_{Nn} in the Arctic region has been described in previous studies that have found that SAI is less efficient during polar nights (Aswathy et al., 2015). In contrast to our results, they found that MSB also is not efficient in lowering T_{Nn} in the Arctic. However, in their experiment they limited the area of increased sea salt aerosols emissions to the atmosphere to the latitudes between 30°S and 30°N while in the modelling output used in this study, this area is increased to latitudes between 45°S and 45°N.

Since MSB is not applied over or close to the Arctic region, we do not expect a difference in shortwave cloud forcing in high-latitudes compared to the other RFG methods which is confirmed by our results. While SAI does target shortwave radiation as well, the mechanism is based on increased aerosol optical depth in the stratosphere and not on cloud albedo, hence no difference in shortwave cloud forcing is expected directly from the treatment either. Our result does show a significant decrease in incoming clear-sky shortwave radiation in the Arctic region for SAI, implying an increase in the amount of diffuse radiation. The positive sign in shortwave radiation in SAI signifies a surface cooling effect through a decreased incoming shortwave flux. The effect of the aerosols on the radiation becomes clearer when looking at the changes in the surface albedo of the three RFG scenarios in the Arctic where SAI is very similar to RCP8.5 while both

CCT and MSB show a decrease. This difference in albedo is a possible explanation as to why SAI shows such different features as compared to CCT and MSB as it leads to less incoming shortwave radiation compared to the other scenarios, offsetting the effect of plant physiological forcing, and hence decreasing the warming and risk for heat waves that we hypothesised for CCT and MSB.

Our results show that under similar global warming (i.e. here 2°C relative to pre-industrial temperatures), RFG leads to climatic conditions increasing fire frequency in CCT and MSB while under SAI, temperature conditions are less favourable for permafrost to occur than under RCP8.5. While we did not look into how fire ignition (e.g. lightning or human-caused ignition) might change under RFG, the shift in climatic conditions is an indication for increased fire activity in the Arctic under CCT and MSB. Both wildfires (Mccarty et al., 2021) and permafrost thawing (Schuur et al., 2008) are huge sources of carbon which when released to the atmosphere will cause further greenhouse gas-driven warming. Hence, it is crucial to understand how the conditions for extreme events will change under RFG management.

In CCT, we see a strengthened hydrological cycle and increased latent heat in the Arctic region, contrary to the other two RFG techniques. This has also been found by Kristjánsson et al. (2015) who could attribute this to the fact that CCT acts on the longwave instead of the shortwave radiation. This can overcompensate for the effect of increased CO_2 concentrations where less precipitation and more droughts are to be expected. CCT, however, holds the danger of overseeding the clouds and thickening them, leading to the opposite effect - increased temperatures and a weakened hydrological cycle (Kristjánsson et al., 2015). As demonstrated by Storelvmo et al. (2013), the desired effect of CCT is only achieved within an optimal range of seeding particle concentrations and premature implementation of CCT could accelerate global warming instead of slowing it down. Similar to CCT, MSB also holds the risk where emitting the wrong particle size or amount could lead to a warming effect by thinning out marine clouds and decreasing the albedo (Alterskjær and Kristjánsson, 2013). One of the most discussed aspects in relation to RFG is the effect of abrupt termination. While not the focus of this thesis, many previous studies have looked into the termination-shock of RFG and concluded that sudden termination of RFG would cause unprecedented changes in temperature (e.g. Jones et al. (2009), Lee et al. (2021), Trisos et al. (2018)). The implementation of RFG would require a globally inclusive governance and conflicts might arise due to countries having different preferred temperatures (Abatayo et al., 2020). Further, it is feared that once RFG is implemented it would reduce the drive for climate change mitigation and adaptation efforts

as it might be seen as the easier option (Lin, 2013). As is already observed with climate change today, the Arctic with its ecosystems and indigenous people would again be over proportionally, negatively affected by RFG, compensating for lower warming rates in the lower latitudes.

The RFG methods evaluated here are currently not understood enough to advocate for practical implementation. Many studies highlight the uncertainties and risks that come with their implementation. We found that whilst RFG methods could effectively cool down the Earth's mean temperature, they show undesirable side effects such as changes to precipitation patterns and extreme temperatures and thus must be handled with care. Further, we have shown in this study, that RFG is not a solution to climate change in the Arctic, a region of major importance for the global climate. It has to be noted that we only used one Earth System Model in our study. The assessment of the impact of plant physiological forcing under RFG would greatly benefit by including the comparison of multiple Earth System Models.

There is no clear estimation for the costs of an actual RFG implementation, as it would have to be carried out for as long as it takes to reduce the CO_2 concentration in the atmosphere. Without reducing the CO_2 in the atmosphere, RFG would have to be continued forever as a sudden stop would cause the climate to rapidly revert to that without RFG methods, leaving no time for ecosystems to adapt. As RFG itself does not alter the atmospheric CO_2, problems caused by increasing CO_2 levels, such as ocean acidification and increased plant physiological forcing, would not be alleviated by RFG. Future research is needed to understand the influence of RFG on climate extremes in ecosystems and how it impacts the socio-economical system. With the current lack of knowledge and the additional negative side effects found in ESMs discussed here, an implementation of RFG is not recommended.

This thesis analysed and showed the side effects of RFG on the Arctic region and highlights why RFG should not be seen as a solution to mitigate the effect of increasing global temperatures due to human-caused climate change.

5 References

Abatayo, A. L., Bosetti, V., Casari, M., Ghidoni, R., and Tavoni, M. (2020). Solar geoengineering may lead to excessive cooling and high strategic uncertainty. *Proceedings of the National Academy of Sciences of the United States of America*, 117(24):13393–13398, DOI: 10.1073/pnas.1916637117.

Ahlm, L., Jones, A., Stjern, W. C., Muri, H., Kravitz, B., and Kristjánsson, J. E. (2017). Marine cloud brightening - As effective without clouds. *Atmospheric Chemistry and Physics*, 17(21):13071–13087, DOI: 10.5194/acp-17-13071-2017.

Ainsworth, E. A. and Long, S. P. (2005). What have we learned from 15 years of free-air CO2 enrichment (FACE)? A meta-analytic review of the responses of photosynthesis, canopy properties and plant production to rising CO2. *New Phytologist*, 165(2):351–372, DOI: 10.1111/j.1469-8137.2004.01224.x.

Akbari, H., Menon, S., and Rosenfeld, A. (2009). Global cooling: Increasing world-wide urban albedos to offset CO2. *Climatic Change*, 94(3-4):275–286, DOI: 10.1007/s10584-008-9515-9.

Alterskjær, K. and Kristjánsson, J. E. (2013). The sign of the radiative forcing from marine cloud brightening depends on both particle size and injection amount. *Geophysical Research Letters*, 40(1):210–215, DOI: 10.1029/2012GL054286.

Aswathy, V. N., Boucher, O., Quaas, M., Niemeier, U., Muri, H., Mülmenstädt, J., and Quaas, J. (2015). Climate extremes in multi-model simulations of stratospheric aerosol and marine cloud brightening climate engineering. *Atmospheric Chemistry and Physics*, 15(16):9593–9610, DOI: 10.5194/acp-15-9593-2015.

Bala, G., Caldeira, K., Nemani, R., Cao, L., Ban-Weiss, G., and Shin, H. J. (2011). Albedo enhancement of marine clouds to counteract global warming: Impacts on the hydrological cycle. *Climate Dynamics*, 37(5):915–931, DOI: 10.1007/s00382-010-0868-1.

Benduhn, F. and Lawrence, M. G. (2013). An investigation of the role of sedimentation for stratospheric solar radiation management. *Journal of Geophysical Research Atmospheres*, 118(14), DOI: 10.1002/jgrd.50622.

Bentsen, M., Bethke, I., Debernard, J. B., Iversen, T., Kirkevåg, A., Seland, Ø., Drange, H., Roelandt, C., Seierstad, I. A., Hoose, C., and Kristjánsson, J. E. (2013). The

Norwegian Earth System Model, NorESM1-M – Part 1: Description and basic evaluation of the physical climate. *Geoscientific Model Development*, 6(3):687–720, DOI: 10.5194/gmd-6-687-2013.

Berdahl, M., Robock, A., Ji, D., Moore, J. C., Jones, A., Kravitz, B., and Watanabe, S. (2014). Arctic cryosphere response in the geoengineering model intercomparison project G3 and G4 scenarios. *Journal of Geophysical Research*, 119(3):1308–1321, DOI: 10.1002/2013JD020627.

climeworks (2021). Climeworks begins operations of Orca, the world's largest direct air capture and CO2 storage plant. *https://climeworks.com/news/climeworks-launches-orca, Last Access Date: 28.07.2022.*

Crook, J. A., Jackson, L. S., Osprey, S. M., and Forster, P. M. (2015). A comparison of temperature and precipitation responses to different Earth radiation management geoengineering schemes. *Journal of Geophysical Research*, 120(18):9352–9373, DOI: 10.1002/2015JD023269.

Crutzen, P. J. (2006). Albedo enhancement by stratospheric sulfur injections: A contribution to resolve a policy dilemma? *Climatic Change*, 77(3-4):211–219, DOI: 10.1007/s10584-006-9101-y.

Da-Allada, C. Y., Baloïtcha, E., Alamou, E. A., Awo, F. M., Bonou, F., Pomalegni, Y., Biao, E. I., Obada, E., Zandagba, J. E., Tilmes, S., and Irvine, P. J. (2020). Changes in West African summer monsoon precipitation under stratospheric aerosol geoengineering. *Earth's Future*, 8(7):e2020EF001595, DOI: 10.1029/2020EF001595.

Davidson, P., Burgoyne, C., Hunt, H., and Causier, M. (2012). Lifting options for stratospheric aerosol geoengineering: Advantages of tethered balloon systems. *Philosophical Transactions of the Royal Society A: Mathematical, Physical and Engineering Sciences*, 370(1974), DOI: 10.1098/rsta.2011.0639.

Drake, B. G., Gonzàlez-Meler, M. A., and Long, S. P. (1997). More efficient plants: A consequence of rising atmospheric CO2? *Annual Review of Plant Biology*, 48:609–639, DOI: 10.1146/annurev.arplant.48.1.609.

Fan, Y., Tjiputra, J., Muri, H., Lombardozzi, D., Park, C. E., Wu, S., and Keith, D. (2021). Solar geoengineering can alleviate climate change pressures on crop yields. *Nature Food*, 2(5):373–381, DOI: 10.1038/s43016-021-00278-w.

Fountain, H. (2021). Test Flight for Sunlight-Blocking Research Is Canceled. *New York Times, https://www.nytimes.com/2021/04/02/climate/solar-geoengineering-block-sunlight.html, Last Access Date: 09.08.2022*, DOI: https://doi.org/10.5067/MODIS/MCD64A1.006.

Geiges, A., Nauels, A., Yanguas Parra, P., Andrijevic, M., Hare, W., Pfleiderer, P., Schaeffer, M., and Schleussner, C. F. (2020). Incremental improvements of 2030 targets insufficient to achieve the Paris Agreement goals. *Earth System Dynamics*, 11(3):697–708, DOI: 10.5194/esd-11-697-2020.

Giglio, L., Justice, C., Boschetti, L., and Roy, D. (2015). MCD64A1 MODIS/Terra+Aqua Burned Area Monthly L3 Global 500m SIN Grid V006 [Data set]. *NASA EOSDIS Land Processes DAAC*, DOI: 10.5067/MODIS/MCD64A1.006.

IPCC (2022). AR6 climate change 2022: Impacts, adaptation and vulnerability. *Contribution of Working Group II to the Sixth Assessment Report of the Intergovernmental Panel on Climate Change*.

Jain, P., Castellanos-Acuna, D., Coogan, S. C., Abatzoglou, J. T., and Flannigan, M. D. (2022). Observed increases in extreme fire weather driven by atmospheric humidity and temperature. *Nature Climate Change*, 12(1):63–70, DOI: 10.1038/s41558-021-01224-1.

Jolly, W. M., Cochrane, M. A., Freeborn, P. H., Holden, Z. A., Brown, T. J., Williamson, G. J., and Bowman, D. M. (2015). Climate-induced variations in global wildfire danger from 1979 to 2013. *Nature Communications*, 6:7537, DOI: 10.1038/ncomms8537.

Jones, A., Haywood, J., and Boucher, O. (2009). Climate impacts of geoengineering marine stratocumulus clouds. *Journal of Geophysical Research*, 114(10):D10106, DOI: 10.1029/2008JD011450.

Jones, A., Haywood, J. M., Alterskjær, K., Boucher, O., Cole, J. N., Curry, C. L., Irvine, P. J., Ji, D., Kravitz, B., Egill Kristjánsson, J., Moore, J. C., Niemeier, U., Robock, A., Schmidt, H., Singh, B., Tilmes, S., Watanabe, S., and Yoon, J. H. (2013). The impact of abrupt suspension of solar radiation management (termination effect) in experiment G2 of the Geoengineering Model Intercomparison Project (GeoMIP). *Journal of Geophysical Research Atmospheres*, 118(17):9743–9752, DOI: 10.1002/jgrd.50762.

Jones, A. C., Haywood, J. M., Dunstone, N., Emanuel, K., Hawcroft, M. K., Hodges, K. I., and Jones, A. (2017). Impacts of hemispheric solar geoengineering on tropical cyclone frequency. *Nature Communications*, 8(1), DOI: 10.1038/s41467-017-01606-0.

Kala, J., De Kauwe, M. G., Pitman, A. J., Medlyn, B. E., Wang, Y. P., Lorenz, R., and Perkins-Kirkpatrick, S. E. (2016). Impact of the representation of stomatal conductance on model projections of heatwave intensity. *Scientific Reports*, 6:23418, DOI: 10.1038/srep23418.

Keller, D. P., Feng, E. Y., and Oschlies, A. (2014). Potential climate engineering effectiveness and side effects during a high carbon dioxide-emission scenario. *Nature Communications*, 5:3304, DOI: 10.1038/ncomms4304.

Kellogg, W. W. and Schneider, S. H. (1974). Climate stabilization: For better or for worse? *Science*, 186(4170):1163–1172, DOI: 10.1126/science.186.4170.1163.

Kharuk, V. I., Ponomarev, E. I., Ivanova, G. A., Dvinskaya, M. L., Coogan, S. C. P., and Flannigan, M. D. (2021). Wildfires in the Siberian taiga. *Ambio*, 50:1953–1974, DOI: 10.1007/s13280.

Kim, J.-S., Kug, J.-S., Jeong, S., Yoon, J.-H., Zeng, N., Hong, J., Jeong, J.-H., Zhao, Y., Chen, X., Williams, M., Ichii, K., and Schaepman-Strub, G. (2022). Arctic warming-induced cold damage to East Asian terrestrial ecosystems. *Communications Earth & Environment*, 3(16), DOI: 10.1038/s43247-022-00343-7.

Kim, J. S., Kug, J. S., Jeong, S. J., Huntzinger, D. N., Michalak, A. M., Schwalm, C. R., Wei, Y., and Schaefer, K. (2017). Reduced North American terrestrial primary productivity linked to anomalous Arctic warming. *Nature Geoscience*, 10(8):572–576, DOI: 10.1038/NGEO2986.

Kirkevåg, A., Iversen, T., Seland, Ø., Hoose, C., Kristjánsson, J. E., Struthers, H., Ekman, A. M. L., Ghan, S., Griesfeller, J., Nilsson, E. D., and Schulz, M. (2013). Aerosol–climate interactions in the Norwegian Earth System Model – NorESM1-M. *Geoscientific Model Development*, 6(1), DOI: 10.5194/gmd-6-207-2013.

Koenigk, T., Key, J., and Vihma, T. (2020). Climate Change in the Arctic. In *Kokhanovsky, A., Tomasi, C. (eds) Physics and Chemistry of the Arctic Atmosphere*. Springer Polar Sciences. Springer, Cham, ISBN: 978-3-030-33566-3, DOI: 10.1007/978-3-030-33566-3.

Kristjánsson, J. E., Muri, H., and Schmidt, H. (2015). The hydrological cycle response to cirrus cloud thinning. *Geophysical Research Letters*, 42(24):10807–10815, DOI: 10.1002/2015GL066795.

Lammertsma, E. I., De Boer, H. J., Dekker, S. C., Dilcher, D. L., Lotter, A. F., and Wagner-Cremer, F. (2011). Global CO2 rise leads to reduced maximum stomatal conductance in Florida vegetation. *Proceedings of the National Academy of Sciences of the United States of America*, 108(10):4035–4040, DOI: 10.1073/pnas.1100371108.

Latham, J. (1990). Control of global warming? *Nature*, 347(6291):339–340, DOI: 10.1038/347339b0.

Latham, J. (2002). Amelioration of global warming by controlled enhancement of the albedo and longevity of low-level maritime clouds. *Atmospheric Science Letters*, 3(2-4), DOI: 10.1006/asle.2002.0048.

Latham, J., Rasch, P., Chen, C. C., Kettles, L., Gadian, A., Gettelman, A., Morrison, H., Bower, K., and Choularton, T. (2008). Global temperature stabilization via controlled albedo enhancement of low-level maritime clouds. *Philosophical Transactions of the Royal Society A: Mathematical, Physical and Engineering Sciences*, 366(1882):3969–3987, DOI: 10.1098/rsta.2008.0137.

Lauvset, K. S., Tjiputra, J., and Muri, H. (2017). Climate engineering and the ocean: Effects on biogeochemistry and primary production. *Biogeosciences*, 14(24):5675–5691, DOI: 10.5194/bg-14-5675-2017.

Lawrence, M. G., Schäfer, S., Muri, H., Scott, V., Oschlies, A., Vaughan, N. E., Boucher, O., Schmidt, H., Haywood, J., and Scheffran, J. (2018). Evaluating climate geoengineering proposals in the context of the Paris Agreement temperature goals. *Nature Communications*, 9(1):3734, DOI: 10.1038/s41467-018-05938-3.

Lee, H., Ekici, A., Tjiputra, J., Muri, H., Chadburn, S. E., Lawrence, D. M., and Schwinger, J. (2019). The response of permafrost and high-latitude ecosystems under large-scale stratospheric aerosol injection and its termination. *Earth's Future*, 7(6):605–614, DOI: 10.1029/2018EF001146.

Lee, H., Muri, H., Ekici, A., Tjiputra, J., and Schwinger, J. (2021). The response of terrestrial ecosystem carbon cycling under different aerosol-based radiation management geoengineering. *Earth System Dynamics*, 12(1):313–326, DOI: 10.5194/esd-12-313-2021.

Lin, A. C. (2013). Does Geoengineering Present a Moral Hazard? *Ecology Law Quarterly*, 40(3):673–712, DOI: 10.15779/Z38JP1J.

MacMartin, D. G., Ricke, K. L., and Keith, D. W. (2018). Solar geoengineering as part of an overall strategy for meeting the 1.5°C Paris target. *Philosophical Transactions of the Royal Society A: Mathematical, Physical and Engineering Sciences*, 376(2119):20160454, DOI: 10.1098/rsta.2016.0454.

Mccarty, J. L., Aalto, J., Paunu, V. V., Arnold, S. R., Eckhardt, S., Klimont, Z., Fain, J. J., Evangeliou, N., Venäläinen, A., Tchebakova, N. M., Parfenova, E. I., Kupiainen, K., Soja, A. J., Huang, L., and Wilson, S. (2021). Reviews and syntheses: Arctic fire regimes and emissions in the 21st century. *Biogeosciences*, 18(18):5053–5083, DOI: 10.5194/bg-18-5053-2021.

McClellan, J., Keith, D. W., and Apt, J. (2012). Cost analysis of stratospheric albedo modification delivery systems. *Environmental Research Letters*, 7(3), ISSN: 17489326, DOI: 10.1088/1748-9326/7/3/034019.

Miralles, D. G., Teuling, A. J., Van Heerwaarden, C. C., and De Arellano, J. V. G. (2014). Mega-heatwave temperatures due to combined soil desiccation and atmospheric heat accumulation. *Nature Geoscience*, 7(5):345–349, DOI: 10.1038/ngeo2141.

Mitchell, D. L. and Finnegan, W. (2009). Modification of cirrus clouds to reduce global warming. *Environmental Research Letters*, 4:045102, DOI: 10.1088/1748-9326/4/4/045102.

Morrow, D. R. (2020). A mission-driven research program on solar geoengineering could promote justice and legitimacy. *Critical Review of International Social and Political Philosophy*, 23(5):618–640, DOI: 10.1080/13698230.2020.1694220.

Muri, H., Kristjánsson, J. E., Storelvmo, T., and Pfeffer, M. A. (2014). The climatic effects of modifying cirrus clouds in a climate engineering framework. *Journal of Geophysical Research*, 119(7):4174–4191, DOI: 10.1002/2013JD021063.

Muri, H., Niemeier, U., and Kristjánsson, J. E. (2015). Tropical rainforest response to marine sky brightening climate engineering. *Geophysical Research Letters*, 42(8):2951–2960, DOI: 10.1002/2015GL063363.

Muri, H., Tjiputra, J., Otterå, O. H., Adakudlu, M., Lauvset, S. K., Grini, A., Schulz, M., Niemeier, U., and Kristjánsson, J. E. (2018). Climate response to aerosol geo-

engineering: A multimethod comparison. *Journal of Climate*, 31(16):6319–6340, DOI: 10.1175/JCLI-D-17-0620.1.

Niemeier, U., Schmidt, H., and Timmreck, C. (2011). The dependency of geoengineered sulfate aerosol on the emission strategy. *Atmospheric Science Letters*, 12(2), DOI: 10.1002/asl.304.

Obu, J., Westermann, S., Barboux, C., Bartsch, A., Delaloye, R., Grosse, F., Heim, B., Hugelius, G., Irrgang, A., Kääb, A. M., Kroisleitner, C., Matthes, H., Nitze, I., Pellet, C., Seifert, F. M., Strozzi, T., Wegmüller, U., Wieczorek, M., and Wiesmann, A. (2021). ESA Permafrost Climate Change Initiative (Permafrost_cci): Permafrost extent for the Northern Hemisphere, v3.0. *NERC EDS Centre for Environmental Data Analysis*, DOI: 10.5285/6e2091cb0c8b4106921b63cd5357c97c.

Park, C. and Allaby, M. (2007). *A Dictionary of Environment and Conservation (1 ed.)*. Oxford University Press, ISBN: 9780198609957, DOI: 10.1093/acref/9780199641666.001.0001.

Park, C. E., Jeong, S. J., Fan, Y., Tjiputra, J., Muri, H., and Zheng, C. (2019). Inequal responses of drylands to radiative forcing geoengineering methods. *Geophysical Research Letters*, 46(23):14011–14020, DOI: 10.1029/2019GL084210.

Park, S.-W., Kim, J.-S., and Kug, J.-S. (2020). The intensification of Arctic warming as a result of CO2 physiological forcing. *Nature Communications*, 11:2098, DOI: 10.1038/s41467-020-15924-3.

Riahi, K., Schaeffer, R., Arango, J., Calvin, K., Guivarch, C., Hasegawa, T., Jiang, K., Kriegler, R., Matthews, R., Peters, G. P., Rao, A., Robertson, S., Sebbit, A. M., Steinberger, J., Tavoni, M., and van Vuuren, D. P. (2022). Mitigation pathways compatible with long-term goals. In *IPCC, 2022: Climate Change 2022: Mitigation of Climate Change. Contribution of Working Group III to the Sixth Assessment Report of the Intergovernmental Panel on Climate Change*. Cambridge University Press, Cambridge, UK and New York, NY, USA, DOI: 10.1017/9781009157926.005.

Ridgwell, A., Singarayer, J. S., Hetherington, A. M., and Valdes, P. J. (2009). Tackling Regional Climate Change By Leaf Albedo Bio-geoengineering. *Current Biology*, 19(2):146–150, DOI: 10.1016/j.cub.2008.12.025.

Roelfsema, M., van Soest, H. L., Harmsen, M., van Vuuren, D. P., Bertram, C., den Elzen, M., Höhne, N., Iacobuta, G., Krey, V., Kriegler, E., Luderer, G., Riahi, K.,

Ueckerdt, F., Després, J., Drouet, L., Emmerling, J., Frank, S., Fricko, O., Gidden, M., Humpenöder, F., Huppmann, D., Fujimori, S., Fragkiadakis, K., Gi, K., Keramidas, K., Köberle, A. C., Aleluia Reis, L., Rochedo, P., Schaeffer, R., Oshiro, K., Vrontisi, Z., Chen, W., Iyer, G. C., Edmonds, J., Kannavou, M., Jiang, K., Mathur, R., Safonov, G., and Vishwanathan, S. S. (2020). Taking stock of national climate policies to evaluate implementation of the Paris Agreement. *Nature Communications*, 11(1):2096, DOI: 10.1038/s41467-020-15414-6.

Russell, L. M., Rasch, P. J., Mace, G. M., Jackson, R. B., Shepherd, J., Liss, P., Leinen, M., Schimel, D., Vaughan, N. E., Janetos, A. C., Boyd, P. W., Norby, R. J., Caldeira, K., Merikanto, J., Artaxo, P., Melillo, J., and Morgan, M. G. (2012). Ecosystem Impacts of Geoengineering: A Review for Developing a Science Plan. *Ambio*, 41(4):350–369, DOI: 10.1007/s13280-012-0258-5.

Salter, S., Sortino, G., and Latham, J. (2008). Sea-going hardware for the cloud albedo method of reversing global warming. *Philosophical Transactions of the Royal Society A: Mathematical, Physical and Engineering Sciences*, 366(1882):3989–4006, DOI: 10.1098/rsta.2008.0136.

Schäfer, S., Irvine, P. J., Hubert, A. M., Reichwein, D., Low, S., Stelzer, H., Maas, A., and Lawrence, M. G. (2013). Correspondence: Field Tests of Solar Climate Engineering. *Nature Climate Change*, 3(9):766, DOI: 10.1038/nclimate1987.

Schuur, E. A., Bockheim, J., Canadell, J. G., Euskirchen, E., Field, C. B., Goryachkin, S. V., Hagemann, S., Kuhry, P., Lafleur, P. M., Lee, H., Mazhitova, G., Nelson, F. E., Rinke, A., Romanovsky, V. E., Shiklomanov, N., Tarnocai, C., Venevsky, S., Vogel, J. G., and Zimov, S. A. (2008). Vulnerability of permafrost carbon to climate change: Implications for the global carbon cycle. *BioScience*, 58(8):701–714, DOI: 10.1641/B580807.

Schuur, E. A., McGuire, A. D., Schädel, C., Grosse, G., Harden, J. W., Hayes, D. J., Hugelius, G., Koven, C. D., Kuhry, P., Lawrence, D. M., Natali, S. M., Olefeldt, D., Romanovsky, V. E., Schaefer, K., Turetsky, M. R., Treat, C. C., and Vonk, J. E. (2015). Climate change and the permafrost carbon feedback. *Nature*, 520(7546):171–179, DOI: 10.1038/nature14338.

Seneviratne, S. I., Corti, T., Davin, E. L., Hirschi, M., Jaeger, E. B., Lehner, I., Orlowsky, B., and Teuling, A. J. (2010). Investigating soil moisture-climate interac-

tions in a changing climate: A review. *Earth-Science Reviews*, 99:125–161, DOI: 10.1016/j.earscirev.2010.02.004.

Seneviratne, S. I., Donat, M. G., Pitman, A. J., Knutti, R., and Wilby, R. L. (2016). Allowable CO2 emissions based on regional and impact-related climate targets. *Nature*, 529(7587):477–483, DOI: 10.1038/nature16542.

Shepherd, J. (2009). *Geoengineering the climate: science, governance and uncertainty*. The Royal Society, London, ISBN: 978-0-85403-773-5.

Skinner, C. B., Poulsen, C. J., and Mankin, J. S. (2018). Amplification of heat extremes by plant CO2 physiological forcing. *Nature Communications*, 9:1094, DOI: 10.1038/s41467-018-03472-w.

Storelvmo, T., Kristjansson, J. E., Muri, H., Pfeffer, M., Barahona, D., and Nenes, A. (2013). Cirrus cloud seeding has potential to cool climate. *Geophysical Research Letters*, 40(1):178–182, DOI: 10.1029/2012GL054201.

Tilmes, S., Mills, M. J., Niemeier, U., Schmidt, H., Robock, A., Kravitz, B., Lamarque, J. F., Pitari, G., and English, J. M. (2015). A new Geoengineering Model Intercomparison Project (GeoMIP) experiment designed for climate and chemistry models. *Geoscientific Model Development*, 8:43–49, DOI: 10.5194/gmd-8-43-2015.

Tjiputra, J. F., Grini, A., and Lee, H. (2016). Impact of idealized future stratospheric aerosol injection on the large-scale ocean and land carbon cycles. *Journal of Geophysical Research: Biogeosciences*, 121(1):2–27, DOI: 10.1002/2015JG003045.

Tjiputra, J. F., Roelandt, C., Bentsen, M., Lawrence, D. M., Lorentzen, T., Schwinger, J., Seland, and Heinze, C. (2013). Evaluation of the carbon cycle components in the Norwegian Earth System Model (NorESM). *Geoscientific Model Development*, 6(2):301–326, DOI: 10.5194/gmd-6-301-2013.

Trisos, C. H., Amatulli, G., Gurevitch, J., Robock, A., Xia, L., and Zambri, B. (2018). Potentially dangerous consequences for biodiversity of solar geoengineering implementation and termination. *Nature Ecology and Evolution*, 2(3):475–482, DOI: 10.1038/s41559-017-0431-0.

UNFCCC (2015). Paris Agreement, Decision1/CP.21.

Vaughan, N. E. and Lenton, T. M. (2011). A review of climate geoengineering proposals. *Climatic Change*, 109(3-4):745–790, DOI: 10.1007/s10584-011-0027-7.

Yoon, J. E., Yoo, K. C., MacDonald, A. M., Yoon, H. I., Park, K. T., Yang, E. J., Kim, H. C., Lee, J. I., Lee, M. K., Jung, J., Park, J., Lee, J., Kim, S., Kim, S. S., Kim, K., and Kim, I. N. (2018). Reviews and syntheses: Ocean iron fertilization experiments - Past, present, and future looking to a future Korean Iron Fertilization Experiment in the Southern Ocean (KIFES) project. *Biogeosciences*, 15(19):5847–5889, DOI: 10.5194/bg-15-5847-2018.

Young, A. M., Higuera, P. E., Duffy, P. A., and Hu, F. S. (2017). Climatic thresholds shape northern high-latitude fire regimes and imply vulnerability to future climate change. *Ecography*, 40(5):606–617, DOI: 10.1111/ecog.02205.

6 Acknowledgement

I want to thank everyone who helped me throughout the process of writing this thesis. First, I would like to thank my supervisors Dr. Jin-Soo Kim and Prof. Gabriela Schaepman-Strub for their help and supervision. I want to thank them for the opportunity to present my work at the World Biodiversity Forum 2022 and for their help with the manuscript sent to Nature Communications. Further, I want to thank the whole SERS group for their continuous support during the process of this thesis. Last, I would like to thank Katharina Müller, Nicolaus Busch, Anouschka Mamie and Lennart Müller for their continuous support and proofreading of my thesis.

7 Appendix

7.1 Linnux PowerShell

The following code was used as a Linux PowerShell to extract single variables from the NorESM1-ME model output.

```
#!/bin/bash
module load daint-gpu
module load CDO

for number in {01,02,03};do

for variable in {FIRE,FLDS,FSA,FSDS,FSDSND,FSDSNI,FSDSVD,FSDSVI,FSH,FSH_G,FSH_V,FSR,QSOIL,QVEGE,QVEGT,RAIN,TBOT,TREFMNAV,TREFMXAV,TSA};do
rm -rf ~/Rhonda/sel_var/${variable}.all.nc


for year in {2020..2100};do

        for month in {01,02,03,04,05,06,07,08,09,10,11,12};do

                        cdo selvar,${variable} NRCP85BPRPEXMSB_${number}.clm2.h0.${year}-${month}.nc temp/${variable}.${number}.${year}-${month}.nc

        done
done

cdo mergetime temp/${variable}.${number}.????-??.nc ~/Rhonda/sel_var/${variable}_${number}_sel_var_MSB.all.nc
done


for variable in {FIRE,FLDS,FSA,FSDS,FSDSND,FSDSNI,FSDSVD,FSDSVI,FSH,FSH_G,FSH_V,FSR,QSOIL,QVEGE,QVEGT,RAIN,TBOT,TREFMNAV,TREFMXAV,TSA};do
        cdo mergetime ~/Rhonda/sel_var/${variable}_${number}_sel_var_MSB.all.nc ~/Rhonda/sel_var/all_selected_variables_${number}_MSB.nc
done
done
```

7.2 Manuscript for Nature Communications

The following pages contain the manuscript submitted to *Nature Communications* in the form it was submitted as, including the extended data.

Radiative forcing geoengineering increases Arctic temperature extremes and permafrost thawing

Rhonda Müller[1,2,*], Jin-Soo Kim[1,*], Hanna Lee[3], Helene Muri[4], Jerry Tjiputra[5], Jin-Ho Yoon[6], Gabriela Schaepman-Strub[1]

[1]Department of Evolutionary Biology and Environmental Studies, University of Zurich, Zurich, Switzerland
[2]Department of Geography, University of Zurich, Zurich, Switzerland
[3]Department of Biology, Norwegian University of Science and Technology, Trondheim, Norway
[4]Industrial Ecology Programme, Department of Energy and Process Engineering, Norwegian University of Science and Technology, Trondheim, Norway
[5]NORCE Norwegian Research Institute, Bjerknes Centre for Climate Research, Bergen, Norway
[6]School of Earth Sciences and Environmental Engineering, Gwangju Institute of Science and Technology, Gwangju, South Korea.

*Corresponding author. Email: rhonda.mueller@uzh.ch and jinsoo.kim@ieu.uzh.ch

Dr. Jin-Soo Kim, Department of Evolutionary Biology and Environmental Studies, University of Zurich, Zurich 8057, Switzerland

Abstract

Radiative forcing geoengineering (RFG) is discussed to be an intermediate solution to partially offset greenhouse gas-driven warming by altering the Earth's energy flows. We show that RFG could exacerbate Arctic temperature extremes in Earth System Model simulations. The three methods including Stratospheric Aerosol Injection, Marine Sky Brightening, and Cirrus Cloud Thinning, mitigate the global mean temperature rise, however, the Arctic warms by 5°C by 2100 under RFG applied to RCP8.5 compared to pre-industrial temperatures. The maximum temperature increase in the Arctic under Cirrus Cloud Thinning and Marine Sky Brightening was primarily attributed to CO_2 plant physiological forcing not controlled by RFG, shifting the system into climatic conditions favoring the development of fires. Under Stratospheric Aerosol Injection, 4.4% of the Arctic land area shifts to temperatures permanently above 0°C, exacerbating permafrost thaw. This study concludes that there may be negative side effects of RFG such as extreme conditions in the Arctic terrestrial systems.

Introduction

In 2015, 196 nations agreed to limit the global mean temperature increase to 2°C – aiming for 1.5°C – in the Paris Agreement treaty[1]. For the first time, global nations united to take action against climate change, which is seen by many as a milestone in the attempts to limit temperature increase on a global scale. However, this requires all countries to accelerate their implementation of policies to reach the required reduction in anthropogenic carbon dioxide (CO_2) emissions. Further there will be a significant emission reduction gap in 2030[2,3], when carbon dioxide (CO_2) emissions should have decreased by 45% compared to 2010[4].

In the meantime, geoengineering is being discussed as an option to partially offset anthropogenic climate warming to buy time. The most common types of geoengineering being discussed are Carbon Dioxide Removal (CDR) and Radiative Forcing Geoengineering (RFG). While CDR aims to remove CO_2 from the atmosphere, for example by enhancing weathering or afforestation, RFG would alter the Earth's radiation budget at the top of the atmosphere (TOA)[5]. Of these two, only CDR addresses the problem at its root by targeting a CO_2 reduction in the atmosphere. However, it would take decades to implement CDR methods on a large scale to be efficient and they require more resources than RFG[5,6,7]. RFG, on the other hand, might be feasible within years and thus scientists argue that it could be useful to rapidly cool the climate for example to keep the Earth system from reaching tipping points[5,7]. However, RFG implementation costs, related to its required continuous deployment, are still debated[5].

Three RFG methods are commonly considered among scientists: Cirrus Cloud Thinning (CCT), Marine Sky Brightening (MSB) and Stratospheric Aerosol Injection (SAI). CCT aims to increase the outgoing longwave radiation at TOA by thinning high

cirrus clouds that reflect longwave radiation back to Earth[8]. MSB and SAI both act on the shortwave radiation budget of the system. In detail, MSB aims to increase cloud coverage and reflection of sunlight over oceans[9,10] and SAI aims to build a layer of aerosols in the stratosphere that scatters part of the incoming solar radiation, increasing the Earth's planetary albedo[11]. All three RFG methods would require a long-term application to keep the global cooling intact[5]. Earth System Models (ESMs) have been used to assess the impacts of large-scale RFG on various aspects of the Earth system to fully understand the feedbacks and consequences of RFG application. Here, we use the Norwegian Earth System Model (NorESM1-ME)[12,13] to understand the responses and feedbacks of terrestrial systems. We use the three most commonly discussed RFG; (i) CCT by increasing the fall speed of ice crystals for temperatures below –38°C, (ii) MSB by increasing the natural emission of sea salt aerosols in the accumulation mode into the atmosphere between the latitudes of 45°S and 45°N, and (iii) SAI by prescribing the properties of an injected layer of sulfur in the stratosphere (see methods or ref.[14]).

While numerous independent studies have confirmed the efficacy of RFG in limiting future global warming, e.g. keeping global mean temperature increase below 2°C[15], others have found undesirable effects on climate conditions and related ecosystem effects under RFG implementation, such as changes in precipitation patterns[16], monsoon periods[17], crop yields[18], altered ocean productivity[19], enhanced ocean acidification[20] and dryland expansion[21]. A few studies have focused on the responses of Arctic ecosystems under RFG (e.g., ref.[22,23]) and there is a lack of thorough analysis on how RFG will impact high-latitude ecosystems. Polar regions have not been the center of attention in the RFG studies due to the short season of impact. We emphasize the importance of polar regions not only due to the amplified climate change they are undergoing, but also due to their climate and ecological teleconnections to mid-

latitudes[24,25], which are fundamental in controlling the Earth's climate[26]. It is crucial to understand the potential side effects of RFG on the Arctic and how RFG might alter the Arctic climate and ecosystems.

RFG would cool the Earth by offsetting the radiative forcing and the greenhouse effect of CO_2 but does not directly downregulate the high CO_2 concentration in the atmosphere. In addition to its greenhouse warming effect, CO_2 also indirectly influences the climate through vegetation feedbacks, with the two main processes being CO_2 fertilization and plant physiological forcing that have opposite effects on transpiration. The CO_2 fertilization effect was found to be dominant over changes in temperature, precipitation and radiation for tropical forests in RFG simulations in ref.[27], generally increasing transpiration of the plants. Plant physiological forcing describes the process of plants closing their stomata under elevated CO_2 concentrations to reduce water loss, hence reducing transpiration[28]. Ref.[29] found that the process of plant physiological forcing in mid- and high-latitudes can remotely influence Arctic temperatures, introducing additional positive feedback and contributing to Arctic amplification. This can lead to changes in extreme temperatures and events such as heatwaves, wildfire frequency, or permafrost thawing. The interplay between intensifying plant physiological forcing under unabated anthropogenic CO_2 emissions and the potential application of RFG in the future is poorly understood and represents a key knowledge gap in RFG research. It is crucial to understand how RFG impacts CO_2 related processes that are not controlled by geoengineering management especially in a region like the Arctic that is not only heavily impacted by plant physiological forcing through heat transport[29] but has also been shown to be one of the most impacted regions by global warming[26].

Here, we assess how RFG methods affect the Arctic, focusing on plant physiological forcing, wildfire frequency, and extreme events, based on the fully interactive Norwegian Earth System Model (NorESM1-ME) simulations (e.g., ref.[14,18,20]). The three RFG methods are implemented in the model such that they reduce the radiative forcing of the representative concentration pathway with 8.5 W m^{-2} radiative forcing (RCP8.5) to 4.5 W m^{-2} (corresponding to the RCP4.5 scenario) by 2100. To analyze extreme events, we assess boreal summer (JJA) maximum temperature (T_{Xx}), boreal winter (DJF) minimum temperature (T_{Nn}) and mean temperature (T_{mean}). Surface warming due to physiological forcing was found to be the highest over mid- to high-latitudes[29], with the excessive surface heat energy being transported to the Arctic region, which is why we analyzed not only the areas > 65°N but also > 50°N. To investigate the impact of plant physiological forcing on temperature extremes in the Arctic, we analyze the regional energy budgets and evaluate potential shifts in the flux partitioning. Lastly, we connect the RFG-induced changes in climatic conditions to Arctic terrestrial system dynamics such as fire frequency and permafrost thawing.

Results

Extreme temperatures increase under RFG in the Arctic

In the region north of 50°N, all three RFG methods and RCP8.5 show similar linear increases of T_{mean} with global mean temperature (T_{glob}, Fig. 1a), indicating an amplified signal as compared to T_{glob}. We show that under RFG (except SAI) the increase in T_{Xx} is even more amplified compared to RCP8.5 north of 50°N indicating stronger intensity of Arctic heatwaves (Fig. 1b), supported by an earlier study[30]. Contrary to T_{Xx}, the three different RFG methods did not show significant difference in T_{Nn} north of 50°N (Fig.

1c). In the land area north of 65°N, T_{Nn} shows the strongest increase per °C increase in T_{glob} under SAI (Supplementary Fig. 1). This result implies that SAI is not as effective in cooling down minimum temperatures in high latitudes.

The spatial pattern of T_{Xx} differences between RFG and RCP8.5 per unit T_{glob} increase (see methods) shows the strongest signals in the Northern Hemisphere under CCT and MSB (Supplementary Fig. 2). This shows that under CCT and MSB, T_{Xx} is increasing more with T_{glob} than under RCP8.5 in mid- and high- northern latitudes. SAI has the smallest deviations from RCP8.5 in T_{Xx}, showing a very similar increase of T_{Xx} with T_{glob} as RCP8.5 (Supplementary Fig. 2). In T_{Nn}, however, SAI is showing different patterns than the other scenarios (Supplementary Fig. 3). While CCT and MSB show some areas where T_{Nn} increases significantly more with T_{glob} than under RCP8.5, other areas show the opposite. With the exception of eastern Siberia and Greenland, SAI shows positive differences to RCP8.5 in all areas north of 50°N.

Change in energy budget components

We expect to see changes in the energy budget as a result of plant physiological forcing due to the effect of closing plant stomata under a high CO_2 concentration environment to save water. As the RFG scenarios do not significantly alter the terrestrial and oceanic carbon sinks[14], they simulate a very similar atmospheric CO_2 increase as RCP8.5, subsequently increasing the effect of plant physiological forcing in the future[31]. Previous studies confirm that plant physiological forcing leads to less transpiration, as the plants close their stomata to preserve water, increasing the ratio of sensible to latent heat and subsequently increasing surface temperatures[28,32,33], explaining the increase in extreme temperatures observed under RFG in the Arctic. We found that the transpiration amount was significantly reduced under all three RFG methods in high-

latitudes relative to RCP8.5 (Fig. 2a, d, g). We also see an increased ratio of sensible to latent heat under all three RFG methods (Fig. 3) which is expected with decreased transpiration and indicates increased plant physiological forcing as compared to RCP8.5.

While we observe reduced transpiration as compared to RCP8.5 during boreal summer in the Arctic under all three RFG methods, an increase in sensible heat is only detected in CCT and MSB (Fig. 2a-i), leading to increased boundary layer temperatures[34,35] and heatwaves[36,37]. Of the three RFG methods, CCT is the only method that shows increased latent heat in the Arctic during the boreal summer (Figs. 2b and 3) indicating a strengthened hydrological cycle[38] which is also illustrated in the precipitation pattern, where CCT shows a general increase in precipitation in the Arctic (Supplementary Fig. 4). Further, this is coherent with the patterns in soil moisture, where CCT shows the largest increase among the RFG methods compared to RCP8.5 (Supplementary Fig. 5). This result is consistent with previous modeling studies that found an increased latent heat flux when applying CCT[38]. While SAI does show an increased ratio of sensible to latent heat during boreal summer - as expected by physiological forcing - sensible heat is decreased as compared to RCP8.5, indicating decreased boundary layer temperatures and explaining why SAI shows a different pattern in T_{Xx} (Fig. 1b).

SAI further shows significant differences to CCT and MSB when considering the shortwave radiation in the Arctic at the time when the scenarios reach the 2°C global mean temperature increase as compared to the pre-industrial temperatures (Fig. 3). While we found a decreased shortwave cloud forcing of similar magnitude in all three RFG scenarios, the clear-sky shortwave radiation significantly differs between them. As MSB is applied in NorESM1 between the latitudes of 45°S and 45°N, we would not

expect an increase in shortwave cloud forcing over the Arctic and we see that shortwave clear-sky radiation in the Arctic is indeed very similar to RCP8.5 (Fig. 3). While SAI does target shortwave radiation as well, the mechanism is based on increased aerosol optical depth in the stratosphere and not on cloud albedo, hence no increased shortwave cloud forcing is expected directly from the treatment either. Our result does show a significant decrease in incoming direct shortwave radiation in the Arctic region for SAI, increasing the amount of diffuse radiation. In Fig. 3, we defined outgoing fluxes as positive while incoming fluxes as negative. Hence, positive fluxes imply a cooling of the Earth's surface, whilst negative imply a warming. The positive sign in shortwave radiation in SAI thus signifies a surface cooling effect through a decreased incoming shortwave flux. The effect of the aerosols on the radiation becomes clearer when looking at the changes in the surface albedo of the three RFG scenarios in the Arctic (Fig. 3). The albedo of SAI in the Arctic during boreal summer is the closest to the one of RCP8.5, not being significantly different, while CCT and MSB show a significant decrease in albedo. This difference in albedo is an explanation as to why SAI shows such different features as compared to CCT and MSB as it leads to less incoming shortwave radiation, offsetting the effect of plant physiological forcing and hence decreasing the warming and risk for heat waves that we hypothesized in Fig. 1b for CCT and MSB.

Impacts on Arctic system dynamics

Last, we assess how shifts in temperature extremes and surface energy budget affect the projected fire frequency and permafrost thawing in the Arctic. Previous studies show that fire frequency increases under hot and dry conditions[39,40,41,42], and Arctic fires are particularly sensitive to boreal summer temperatures[41,42]. We have already shown

that under CCT and MSB, maximum summer temperature increases more with T_{glob} than RCP8.5 and SAI, potentially leading to climatic conditions with more frequent fire activity in the Arctic. Our results show that the majority of fire events occur when T_{Xx} anomalies are higher than T_{mean} anomalies (Fig. 4a), indicating that T_{Xx} is a stronger driver for fire frequency than T_{mean}. The simulated temperature frequency distribution when RCP8.5 reaches 2°C global warming shows that the frequency is highest around when T_{Xx} anomalies are similar to T_{mean} anomalies (Fig. 4b), but under CCT and MSB, their frequencies shift towards regions where T_{Xx} is higher than T_{mean} as compared to where T_{Xx} is lower than T_{mean}(Fig. 4c, d). This means higher T_{Xx} anomalies are simulated under CCT and MSB under given T_{mean} anomalies especially for 3° of T_{mean} anomalies. These conditions are favorable conditions for fire activity as we have shown in Fig. 4a. This result suggests that temperature conditions under CCT and MSB shift towards conditions where fire frequency is higher than under RCP8.5 for the 2°C global mean temperature increase.

Permafrost thawing may accelerate global scale warming by releasing large amounts of organic matter storage[43] as greenhouse gas emissions[44]. We hypothesize that permafrost may continue to thaw more with the strong increase in the minimum temperatures over several years. We focus on SAI to test this hypothesis as SAI is the only scenario where boreal winter minimum temperatures north of 65°N differ from the other scenarios (Supplementary Fig. 1). The current distribution of permafrost fraction against temperature conditions (T_{mean} versus T_{Nn}) shows that the permafrost fraction is highest below −10°C T_{mean} and is more sensitive to T_{Nn} for mid T_{mean} ranges (Fig. 5a). The T_{Nn} frequency distribution of RCP8.5 when the scenario reaches 2°C global warming shows that T_{Nn} generally is below T_{mean}, the maximum frequency region being around −15°C T_{mean} and −30°C T_{Nn} (Fig. 5b). We noticed that the region of the highest

frequency of T_{Nn} conditions shifts towards higher temperatures, where temperature conditions are less favorable for permafrost to occur (Fig. 5c). The maximum difference in T_{Nn} is around −10°C T_{mean}, where the permafrost fraction might be particularly sensitive to T_{Nn}. We found that 29 gridcells north of 65° change from T_{Nn} below 0° in 2006-2026 to above 0° in 2080-2100 in the SAI scenario. This corresponds to 4.4% of the land area north of 65°N or 628 879 km^2. 7.2% of the area changes from T_{mean} below 0° in 2006-2026 to above 0° in 2080-2100. Our results indicate that under SAI, the climatic conditions in the Arctic will be less favorable for permafrost when compared to RCP8.5 when the two scenarios reach the 2° global mean temperature increase.

Implications and Outlook

We show that all three of the presented RFG methods could introduce additional risks to the Arctic terrestrial system at a 2°C global climate warming level. The changes observed in the energy budget components in CCT and MSB support the hypothesis that the increase in T_{Xx} in the Arctic can be linked to plant physiological forcing. At 2°C warming, SAI does not deviate significantly from RCP8.5 in T_{Xx}. While the decrease in transpiration and increase ratio of sensible to latent heat indicates enhanced plant physiological forcing for all three RFG methods, the effect in SAI is potentially offset due to changes in shortwave radiation, leading to higher surface albedo as compared to the other RFG methods (Fig. 3).

Our results show, that under similar global warming (i.e., here 2°C relative to pre-industrial), RFG leads to climatic conditions favoring more fire activities in CCT and MSB while under SAI, temperature conditions are less favorable for permafrost to occur, than under RCP8.5. While we did not look into how fire ignition (e.g., lightning or human-caused ignition) might change under RFG, the shift in climatic conditions is an indication for increased fire activity in the Arctic under CCT and MSB. Both

wildfires[45] and permafrost thawing[43] are huge sources of carbon which is why it is crucial to understand how the conditions for extreme events will change under RFG management.

The RFG methods evaluated here are currently not understood enough to advocate for practical implementation. Many studies highlight the uncertainties and risks that come with implementation. We found that whilst RFG methods could effectively cool down the Earth's mean temperature, they show undesirable side effects such as changes to precipitation patterns and extreme temperatures and thus must be handled with care. It has to be noted that we only used one Earth System Model in our study. The assessment of the impact of plant physiological forcing under RFG would greatly benefit by including the comparison of multiple Earth System Models.

There is no clear estimation for the costs of an actual RFG implementation, as it would have to be carried out for as long as it takes to reduce the CO2 concentration in the atmosphere. Without reducing the CO2 in the atmosphere, RFG would have to be continued forever as a sudden stop would cause the climate to rapidly revert to that without RFG methods[14,21], leaving no time for ecosystems to adapt. Future research is needed to understand the influence of RFG on climate extremes in ecosystems and how it impacts the socio-economical system. With the current lack of knowledge and the additional negative side effects found in ESMs discussed here, an implementation of RFG is not recommended.

Methods

Model description. To assess the influence of RFG on the Arctic terrestrial systems, we use the fully coupled Norwegian Earth System Model (NorESM1-ME) described in detail by ref.[12,13]. Nor-ESM1 is based on the Community Climate System Model version 4 (CCSM4). Changes relevant for this analysis are a modified chemistry-aerosol-cloud-radiation scheme[46] and coupling of the ocean carbon cycle model with an isopycnic ocean general circulation model[13]. The model participated in phase 5 of the Climate Model Intercomparison Project (CMIP5), and the Geoengineering Model Intercomparison Project (GeoMIP). It has a resolution of 1.9° latitude by 2.5° longitude and 26 vertical layers[12]. The variables used in this analysis are summarized in Table 1.

Radiative forcing geoengineering scenarios. Three RFG methods are analyzed here: Cirrus cloud thinning (CCT), marine sky brightening (MSB), and stratospheric aerosol injection (SAI). They are designed such that they reduce the radiative fluxes at the top of the atmosphere from the RCP8.5 levels to that of the RCP4.5 scenario, requiring a radiative forcing of -4 W m^{-2} by 2100. Geoengineering is applied for 81 years, starting in 2020. Three different ensembles are carried out for each scenario, each with a small perturbation to initial conditions in the year 2020[14]. For the RCP8.5 scenario, used as the baseline scenario in this study, one simulation was carried out, running from 2006–2100.

CCT aims to thin out high ice clouds, i.e., cirrus, that act to trap longwave radiation in the climate system and thus have a net warming effect. By thinning these clouds, more longwave radiation can escape to space, altering the Earth's radiation budget. This can be achieved by seeding ice nuclei in regions where cirrus clouds form to initiate heterogeneous freezing and the formation of larger crystals that may fall out of the clouds, thereby thinning them out[8]. In Nor-ESM1, the method by ref.[47] was

implemented: CCT is approximated by increasing the fall speed of crystals for temperatures colder than −38°C, the temperature where typically homogeneous freezing sets in. By increasing the number of particles, heterogeneous freezing can dominate and deplete the clouds of water vapor. The fall speed was increased by a factor of up to 10 by the end of the century.

MSB acts on the shortwave energy budget of the Earth system by enhancing the concentration of droplets in low marine stratocumulus clouds, increasing the cloud albedo. The suggested method is to inject ocean water mist into the lower atmosphere in regions where there is a deficit of cloud condensation nuclei (CCN) where the NaCl would function as CCN[10,48]. The direct effect of the bright sea salt aerosols is also contributing to the cooling in the model, as established in ref.[8]. MSB is implemented in Nor-ESM1 according to the method of ref.[49] by increasing the natural emission of sea salt aerosols in the accumulation mode from the ocean surface to the lower atmosphere between the latitudes of 45°S and 45°N. To achieve the required −4 W m^{-2} in radiative forcing, the ocean area where CCN are emitted was increased as compared to ref.[49] who limited their area to ±30°. By the end of the century, emissions of ~460 Tg yr^{-1} of sea salt were required over the whole area[14].

Similar to MSB, SAI affects the shortwave radiation budget of the Earth. SAI is the most studied radiative forcing geoengineering approach as it is based on the natural dimming following volcanic eruptions. In this approach, aerosols like SO_2 are injected into the stratosphere, building a layer of aerosols that effectively scatter part of the incoming solar radiation, increasing the Earth's planetary albedo[11,50]. The implementation of SAI in Nor-ESM1 is according to the description of ref.[51]: SO_2 is injected into the stratosphere at a grid point close to the equator at a height of around 20-km (60 hPa). The following distribution of the SO_2 was simulated using an

interactive aerosol microphysics module (HAM) of the general circulation model ECHAM5. Ref.[14] found that the needed emission strength to offset 4 W m^{-2} radiative forcing requires 5 Tg(S) yr^{-1} in 2050, increasing to 10 Tg(S) yr^{-1} in 2075 and 20 Tg(S) yr^{-1} in 2100.

Experimental design. Our focus is to compare the RFG methods to the RCP8.5 at the same level of global mean temperature increase. For this we determine for every ensemble, the year they reach the 2°C global mean temperature increase (289.15°K) compared to the pre-industrial mean. We calculated the pre-industrial mean from Nor-ESM1 simulations as the mean of global temperatures from a 500 year control simulation. If not stated otherwise, the data are handled as a 21-year running mean. We calculate anomalies with respect to the mean of the first 21 years of the RCP8.5 scenario (2006–2026). As we are interested in the land processes in the Arctic, most variables are considered only over land. The only exception is global mean temperature (T_{glob}). To calculate the mean over an area, we apply a cosine weighted mean. The ensembles are generally considered as a mean for each RFG method individually. If not stated otherwise, the maximum temperature (T_{Xx}) is calculated as the maximum temperature of the JJA months for each year, minimum temperature (T_{Nn}) as the minimum temperature of the DJF months for each year (December being taken from the year before) and mean temperature (T_{mean}) as the mean temperature of all months of the respective year. We defined albedo as upward / downward shortwave radiation at the surface.

To assess how the Arctic temperature regimes shift under RFG, we analyzed the current (2001 - 2020) observed T_{Xx} and T_{mean} JJA conditions for a satellite data-driven fire frequency dataset (MCD64). We further analyzed the T_{Xx} frequency under RCP8.5 from 2006–2026 to count frequencies under a given mean and maximum

temperature anomalies in the Arctic (Fig. 4b) and how the temperature frequencies shift under CCT and MSB (Fig. 4c, d). We determine the temperature frequencies by making 0.6X0.6°C (Fig. 4) and 2.0X3.0°C (Fig. 5) bins and evaluating how often each T_{Xx}/T_{Nn} and T_{mean} combination is present in all the land grid cells north of 50 and 65°N, respectively, divided by the number of total land grid cells north of 50 and 65°N, respectively. Only grid cells that contain at least 50% of boreal plant function types (needleleaf evergreen boreal tree, needleleaf deciduous boreal tree, broadleaf deciduous boreal tree, broadleaf deciduous boreal shrub, and C3 arctic grass) are considered for the fire plots. We calculate the fire frequency in a similar way by calculating the burned area for the respective temperature conditions from the MCD64 monthly burned area dataset from 2001 to 2020 and the same time frame for the temperature anomalies[52]. As single heat events are important for fires, we consider the JJA months separately for the fire plots, while for the permafrost plots, the DJF months are taken as mean, since longer cold or warm periods are more influential than short events. To determine anomalies, T_{Xx} and T_{mean} are calculated for each grid cell for the RCP8.5 2006–2026 period and subtracted from T_{Xx} and T_{mean} of that grid cell when the scenarios reach the 2°C global mean temperature increase. The permafrost fraction was calculated based on a dataset of the European Space Agency's Climate Change Initiative Permafrost project and covers the period from 2003 to 2019[53]. No anomalies are determined for T_{Nn} as permafrost thawing depends on absolute temperatures and is not anomaly-driven like fires.

Linear regression analysis. To assess the spatial differences between the RFG and the RCP8.5 scenarios we perform a linear regression (LR) analysis. We calculate T_{glob} temperature of each ensemble for the timespan 2006-2100 for RCP8.5 and 2020-2100 for RFG with a cosine weighted mean and a 21-year running mean. In the example of

Fig. 2a, we calculate the JJA mean of transpiration as 21-year running mean for every land grid cell for all three CCT ensembles and the RCP8.5 scenario and evaluate its dependence on the T_{glob} using linear regression. We perform a LR for every land grid cell with T_{glob} as independent and the transpiration of that grid cell as dependent variable for every ensemble. The difference in slope plotted in Fig. 2a represents the difference of the mean slope of the three CCT ensembles and the RCP8.5 slope.

To test for significant differences between CCT and RCP8.5 we calculate the residual of the CCT temperature values once with the results of the LR of RCP8.5 and once with the results of the LR of CCT for each grid cell and comparing those residuals with an unpaired t-test. Assuming there are no differences between CCT and RCP8.5, equation (1) should yield the same result for the LR results for both CCT and RCP8.5:

$$b = T_{Xx,CCT(n)}[i] - slope_{RCP\ or\ CCT(n)} \cdot T_{mean,CCT(n)}[i] - intercept_{RCP\ or\ CCT(n)}, \quad (1)$$

where n = 1, 2, 3, represents the three CCT ensembles, i is for centered year of the 21-year running mean and slope and intercept represent the slope and intercept for RCP8.5 and the three CCT ensembles. Hence, when conducting a t-test for the b-values obtained for the slope and intercept of the RCP8.5 LR and the b-values obtained for the slopes and intercepts of the CCT LRs, p-values <0.05 indicate that there is a significant difference between the LRs of CCT and RCP8.5.

Data and code availability.

The codes used to generate the results and figures of this work are available at github repository (https://github.com/RhondaMueller/Codes-RFG-Arctic-Impacts.git). The NorESM1-ME model is described in detail in ref.[12,13]. The data used to create the figures in this work is available from the github repository (https://github.com/RhondaMueller/Data-RFG-Arctic-Impacts.git).

References

1. UNFCCC. *Paris Agreement, Decision 1/CP.21* (2015).
2. Geiges, A. et al. Incremental improvements of 2030 targets insufficient to achieve the Paris Agreement goals. *Earth Syst. Dyn.* **11,** 697–708 (2020).
3. Roelfsema, M. et al. Taking stock of national climate policies to evaluate implementation of the Paris Agreement. *Nat. Commun.* **11,** 2096 (2020).
4. Riahi, K. et al. Mitigation pathways compatible with long-term goals. In *IPCC, 2022: Climate Change 2022: Mitigation of Climate Change. Contribution of Working Group III to the Sixth Assessment Report of the Intergovernmental Panel on Climate Change*. Cambridge University Press, Cambridge, UK and New York, NY, USA (2022)
5. Lawrence, M. G. et al. Evaluating climate geoengineering proposals in the context of the Paris Agreement temperature goals. *Nat. Commun.* **9,** 3734 (2018).
6. Russell, L. M. et al. Ecosystem impact of geoengineering: A review for developing a science plan. *Ambio* **41,** 350-369 (2012).
7. Shepherd, J. K. et al. *Geoengineering the climate: science, governance and uncertainty* (The Royal Society, London, 2009).
8. Mitchell, D. L. & Finnegan, W. Modification of cirrus clouds to reduce global warming. *Environ. Res. Lett.* **4** (2009).
9. Ahlm, L. et al. Marine cloud brightening - as effective without clouds. *ACP* **17**, 13071-13087 (2017)
10. Latham, J. Control of global warming? *Nature* **347,** 339-340 (1990).
11. Kellogg, W. W. & Schneider, S. H. Climate stabilization: For better or for worse? *Science* **186,** 1163-1172 (1974).

12. Bentsen, M. et al. The Norwegian Earth System Model, Nor-ESM1-M – Part 1: Description and basic evaluation of the physical climate. *Geosci. Model Dev.* **6,** 687-720 (2013).
13. Tjiputra, J. F. et al. Evaluation of the carbon cycle components in the Norwegian Earth System Model (NorESM). *Geosci. Model Dev.* **6,** 301-325 (2013).
14. Muri, H. et al. Climate response to aerosol geoengineering: A multimethod comparison. *J. Clim.* **31,** 6319-6340 (2018).
15. MacMartin, D. G, Ricke, K. L. & Keith, D. W. Solar geoengineering as part of an overall strategy for meeting the 1.5°C Paris target. *Phil. Trans. R. Soc. A.* **376,** 20160454 (2018)
16. Keller, D. P., Feng, E. Y. & Oschlies, A. Potential climate engineering effectiveness and side effects during a high carbon dioxide-emission scenario. *Nat. Commun.* **5,** 3304 (2014).
17. Da-Allada, C. Y. et al. Changes in West African summer monsoon precipitation under stratospheric aerosol geoengineering. *Earth's Future* **8,** e2020EF001595 (2020).
18. Fan, Y. et al. Solar geoengineering can alleviate climate change pressures on crop yields. Nat. Food 2, 373-381 (2021).
19. Lauvset, S. K, Tjiputra, J. F. & Muri, H. Climate engineering and the ocean: effects on biogeochemistry and primary production. *BG* **14**, 5675-5691 (2017).
20. Tjiputra, J. F., Grini, A. & Lee, H. Impact of idealized future stratospheric aerosol injection on the large-scale ocean and land carbon cycles. *J. Geophys. Res. Biogeosci.* **21**, 2-27 (2015).

21. Park, C.-E. et al. Inequal responses of drylands to radiative forcing geoengineering methods. *Geophys. Res. Lett.* **46,** 14011-14020 (2019).
22. Berdahl, M. et al. Arctic cryosphere response in the Geoengineering Model Intercomparison Project G3 and G4 scenarios. *J. Geophys. Res. Atmos.* **119**, 1308-1321 (2014)
23. Lee, H. et al. The response of permafrost and high-latitude ecosystems under large-scale stratospheric aerosol injection and its termination. *Earth's Future* **7,** 605-614 (2019).
24. Kim, J.-S. et al. Reduced North American terrestrial primary productivity linked to anomalous Arctic warming. *Nat*. *Geosci*. **10,** 572-576 (2017).
25. Kim, J.-S. et al. Arctic warming-induced cold damage to East Asian terrestrial ecosystems. *Commun*. *Earth*. *Environ*. **3,** 16 (2022).
26. IPCC. AR6 climate change 2022: Impacts, adaptation and vulnerability (2022).
27. Muri, H., Niemeier, U. & Kristjánsson, J. E. Tropical rainforest response to marine sky brightening climate engineering. *Geophys. Res. Lett*. **42**, 2951-2960 (2015).
28. Drake, B. G., Gonz lez-Meler, M. A. & Long, S. P. More efficient plants: a consequence of rising atmospheric CO_2? *Annu*. *Rev*. *Plant Physiol*. *Plant Mol*. *Biol*. **48,** 609-639 (1997).
29. Park, S.-W., Kim, J.-S. & Kug, J.-S. The intensification of Arctic warming as a result of CO_2 physiological forcing. *Nat. Commun.* **11,** 2098 (2020).
30. Seneviratne, S. I., Donat, M. G., Pitman, A. J., Knutti, R. & Wilby, R. L. Allowable CO_2 emissions based on regional and impact-related climate targets. *Nature* **529,** 477-483 (2016).

31. Lee, H., Muri, H., Ekici, A., Tjiputra, J. & Schwinger. J. The response of terrestrial ecosystem carbon cycling under different aerosol-based radiation management geoengineering. *Earth Syst. Dyn.* **12,** 313-326 (2021).

32. Ainsworth, E. A. & Long, S. P. What have we learned from 15 years of free-air CO_2 enrichment (FACE)? A meta-analytic review of the responses of photosynthesis, canopy properties and plant production to rising CO_2. *N*. *Phytol*. **165,** 351-372 (2005).

33. Lammertsma, E. I. et al. Global CO_2 rise leads to reduced maximum stomatal conductance in Florida vegetation. *Proc*. *Natl*. *Acad*. *Sci*. *USA* **108,** 4035-4040 (2011).

34. Seneviratne, S. I. et al. Investigating soil moisture-climate interactions in a changing climate: A review. *Earth-Sci*. *Rev*. **99,** 125-161 (2010).

35. Miralles, D. G., Teuling, A. J., van Heerwaarden, C. C. & Vila-Guerau de Arellano, J. Mega-heatwave temperatures due to combined soil desiccation and atmospheric heat accumulation. *Nat*. *Geosci*. **7,** 345-349 (2014).

36. Kala, J. et al. Impact of the representation of stomatal conductance on model projections of heatwave intensity. *Sci*. *Rep*. **6,** 23418 (2016).

37. Skinner, C. B., Poulsen, C. J. & Mankin, J. S. Amplification of heat extremes by plant CO_2 physiological forcing. *Nat*. *Commun*. **9,** 1094 (2018).

38. Kristjánsson, J. E., Muri, H. & Schmidt, H. The hydrological cycle response to cirrus cloud thinning. *Geophys. Res. Lett.* **42,** 10807-10815 (2015).

39. Jain, P., Castellanos-Acuna, D., Coogan, S. C. P., Abatzoglou, J. T. & Flannigan, M. D. Observed increases in extreme fire weather driven by atmospheric humidity and temperature. *Nat. Clim. Change* **12,** 63-70 (2022).

40. Jolly, W. M. et al. Climate-induced variations in global wildfire danger from 1979 to 2013. *Nat. Commun.* **6,** 7537 (2015).
41. Kharuk, V. I. et al. Wildfires in the Siberia Taiga. *Ambio* **50,** 1953-1974 (2021).
42. Young, A. M., Higuera, P. E., Duffy, P. A. & Sheng Hu, F. Climatic thresholds shape northern high-latitude fire regimes and imply vulnerability to future climate change. *Ecography* **40,** 606-617 (2017).
43. Schuur, E. A. G. et al. Vulnerability of permafrost carbon to climate change: Implications for the global carbon cycle. *Bioscience* **58,** 701-714 (2008).
44. Schuur, E. A. G. et al. Climate change and the permafrost carbon feedback. *Nature* **520,** 171-179 (2015).
45. McCarty, J. et al. Reviews and syntheses: Arctic fire regimes and emissions in the 21st century. *Biogeosciences* **18**, 5053-5083 (2021).
46. Kirkevåg, A. et al. Aerosol-climate interactions in the Norwegian Earth System Model – NorESM1-M. *Geosci. Model Dev.* **6,** 207-244 (2013).
47. Muri, H., Kristjánsson, J. E., Storelvmo, T. & Pfeffer, M. A. The climatic effects of modifying cirrus clouds in a climate engineering framework. *J. Geophys. Res. Atmos.* **119,** 4174-4191 (2014).
48. Latham, J. Amelioration of global warming by controlled enhancement of the albedo and longevity of low-level maritime clouds. *Atmospheric Sci. Lett.* **3,** 52-58 (2002).
49. Alterskjær, K. & Kristjánsson, J. E. The sign of the radiative forcing from marine cloud brightening depends on both particle size and injection amount. *Geophy. Res. Lett.* **40,** 210-215 (2013).

50. Crutzen, P. J. Albedo enhancement by stratospheric sulfur injections: A contribution to resolve a policy dilemma? *Clim. Change* **77** (2006).
51. Tilmes, S. et al. A new Geoengineering Model Intercomparison Project (GeoMIP) experiment designed for climate and chemistry models. *Geosci. Model Dev.* **8,** 43-49 (2015).
52. Giglio, L., Justice, C., Boschetti, L. & Roy, D. . MCD64A1 MODIS/Terra+Aqua Burned Area Monthly L3 Global 500m SIN Grid V006 [Data set]. *NASA EOSDIS Land Processes DAAC*. (2015). https://doi.org/10.5067/MODIS/MCD64A1.006
53. Obu, J. et al. ESA Permafrost Climate Change Initiative (Permafrost_cci): Permafrost extent for the Northern Hemisphere, v3.0. N*ERC EDS Centre for Environmental Data Analysis* (2021). doi:10.5285/6e2091cb0c8b4106921b63cd5357c97c

Acknowledgments

Author Contributions R. Müller conducted analyses, prepared figures, and wrote the manuscript. R. Müller and J.-S. Kim designed the research and wrote the majority of the manuscript content. H. Muri, H. Lee, and J. Tjiputra provided the output of the NorESM1-ME simulations. R. Müller, J.-S. Kim, H. Muri, H. Lee, J. Tjiputra, J.-H. Yoon, and G. Schaepman-Strub. discussed the results and revised the manuscript.

Competing interests The authors declare no competing interests.

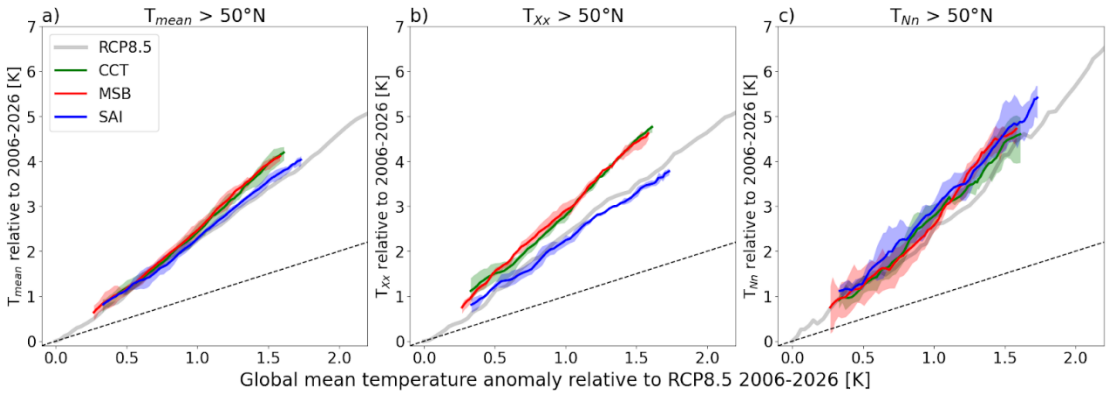

Fig. 1: Simulated temperature change in RCP8.5, CCT, MSB and SAI. a-c, Anomaly in mean (T_{mean}), maximum (T_{Xx}) and minimum (T_{Nn}) land temperature north of 50°N (y-axis) compared to the global mean temperature (T_{glob}) anomaly over land and ocean (x-axis). The anomalies are respective to the mean of RCP8.5 from 2006-2026. The lines represent the ensemble mean. The ensemble spread is shaded. The hatched line represents the 1:1 line.

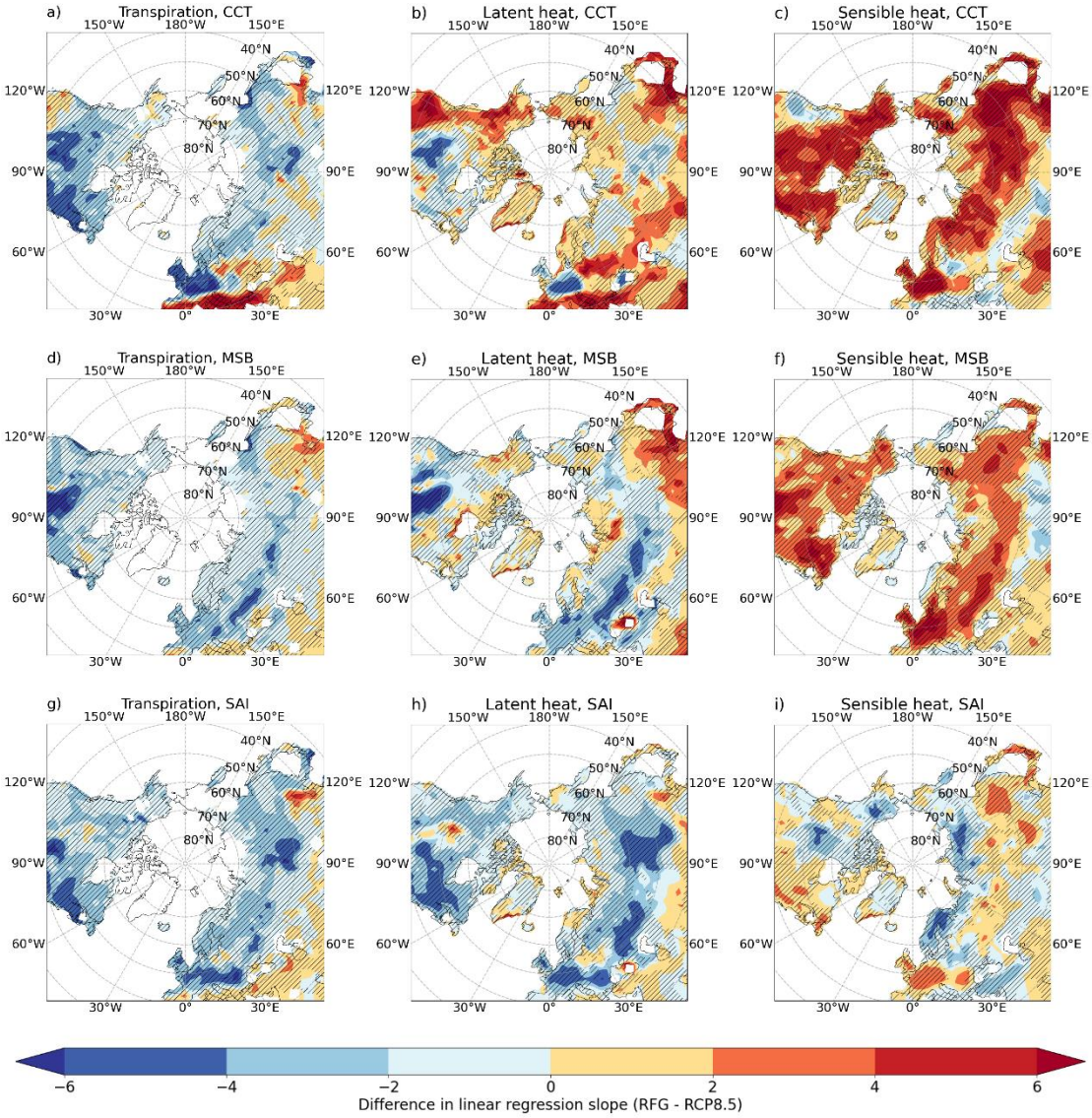

Fig. 2: Simulated change of transpiration, latent heat, and sensible heat in the Arctic for CCT, MSB, and SAI. Pattern of the difference between the respective RFG scenarios and the RCP8.5 scenario in the linear regression slope between transpiration, latent heat, and sensible heat, respectively, and T_{glob}. Areas with a significant difference in slope of RCP8.5 and RFG scenarios are hatched.

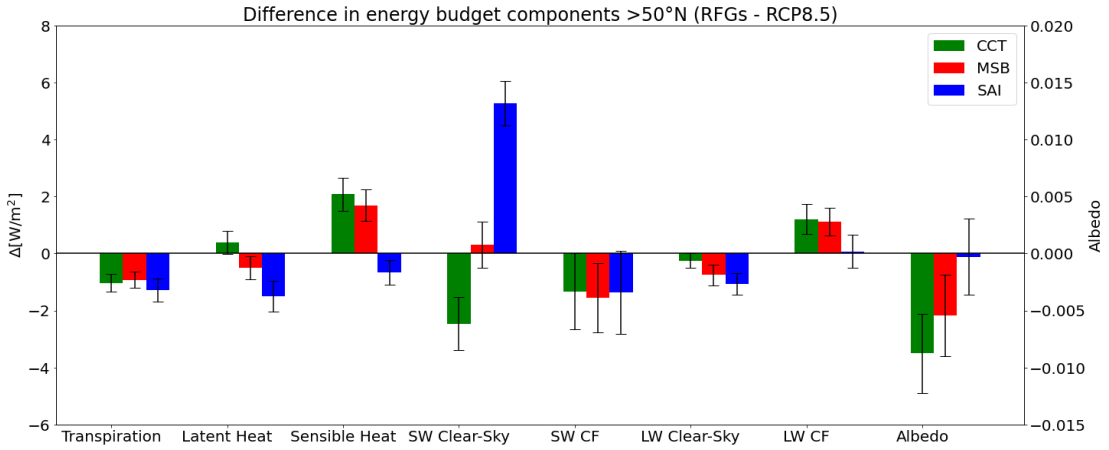

Fig. 3: Change in energy budget components north of 50°N. Difference of the energy budget components >50°N from the initial values from the first 21 years of the RCP8.5 scenario to when each scenario reaches the 2°C global warming as compared to the pre-industrial mean. For albedo, the right y-axis applies; all other variables are plotted on the left y-axis. The skewers indicate 95% confidence intervals. Incoming fluxes are defined as negative, outgoing fluxes as positive. SW = shortwave, LW = longwave, CF = cloud forcing.

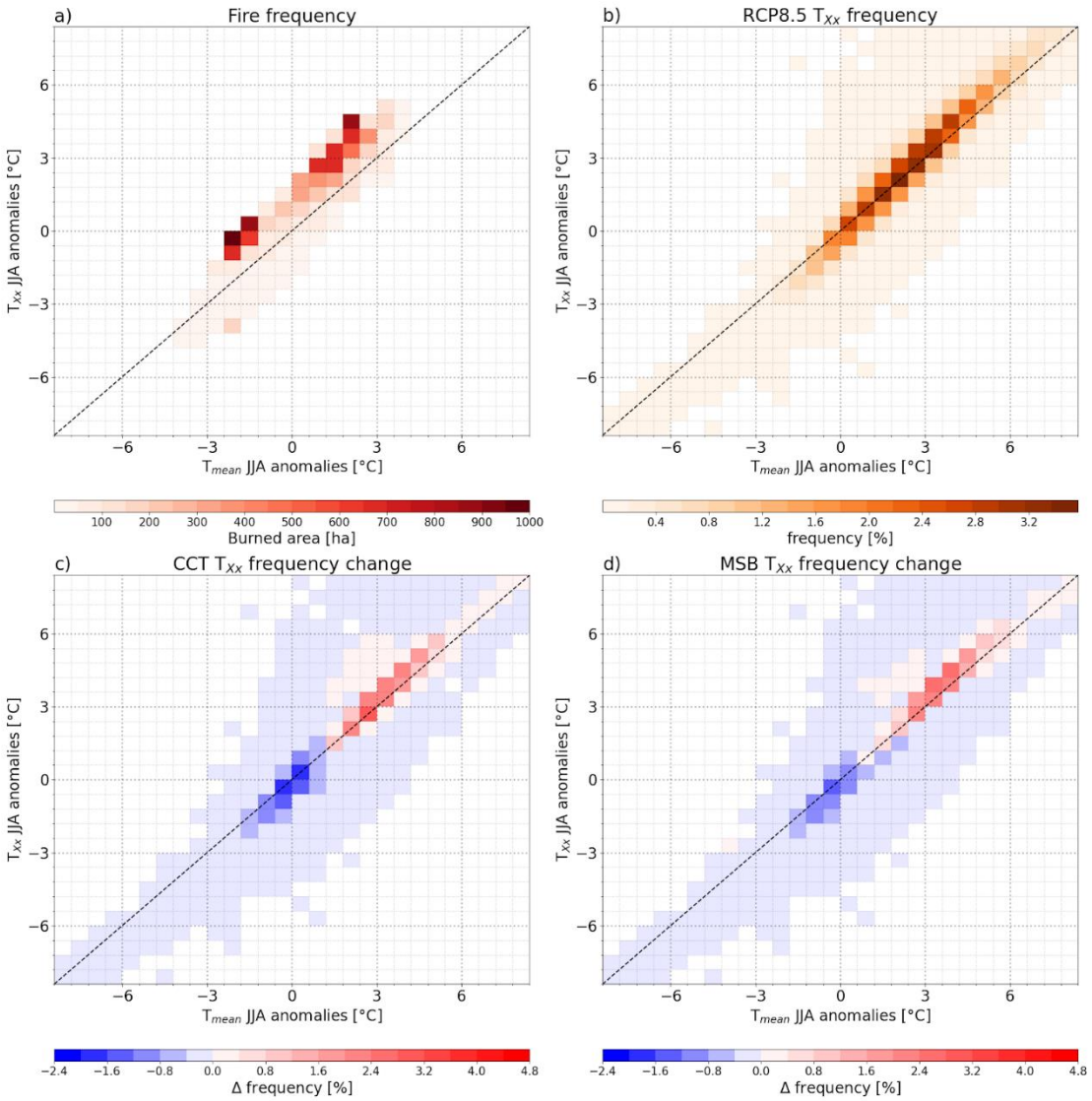

Fig. 4: Change in JJA maximum temperature frequency in CCT and MSB related to fire frequency north of 50°N. a, conditions under which fires are currently observed in the Arctic (Giglio, 2015). The anomalies are calculated to 2001-2020. **b**, maximum temperature frequency north of 50°N when the RCP8.5 scenario reaches 2°C global mean temperature increase as compared to pre-industrial. **c-d**, difference of the maximum temperature frequency between when CCT and MSB reach the 2°C global mean temperature increase and when the RCP8.5 scenario reaches 2°C increase. The hatched line represents the 1:1 line.

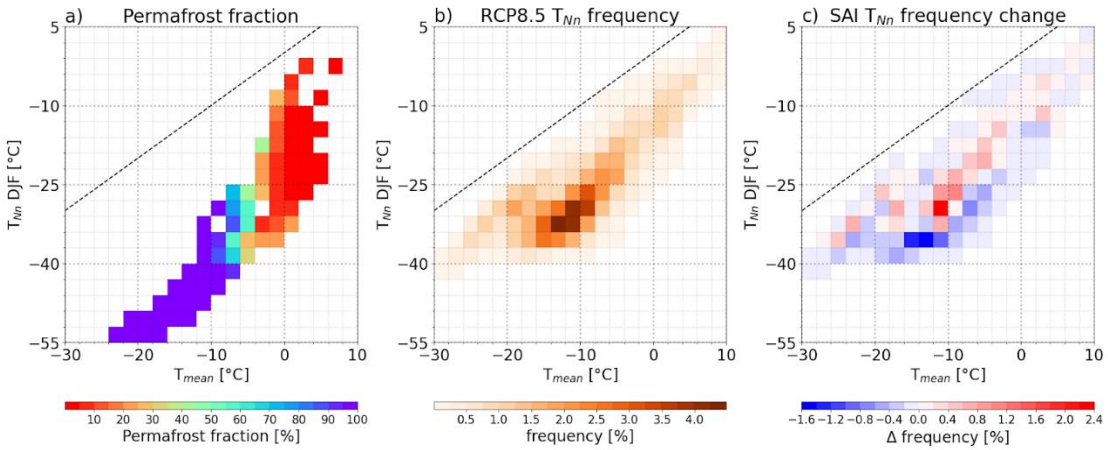

Fig. 5: Change in DJF minimum temperature frequency in SAI related to permafrost north of 65°N. a, conditions under which permafrost is currently observed in the Arctic (Obu, 2021). **b**, minimum temperature frequency north of 65°N when the RCP8.5 scenario reaches 2°C global mean temperature increase as compared to pre-industrial. **c**, difference of the minimum temperature frequency between when SAI reaches the 2°C global mean temperature increase and when the RCP8.5 scenario reaches 2°C increase. The hatched line represents the 1:1 line.

Table 1: Description of the analyzed variables.

Name	Long Name
TS	Surface temperature (radiative) [K]
TREFMXAV	Daily maximum of average 2-m temperature [K]
TREFMNAV	Daily minimum of average 2-m temperature [K]
FCTR	Canopy transpiration [W m^{-2}]
LHFLX	Surface latent heat flux [W m^{-2}]
SHFLX	Surface sensible heat flux [W m^{-2}]
FSNSC	Clearsky net solar flux at surface [W m^{-2}]
FSNS	Net solar flux at surface [W m^{-2}]
FLNSC	Clearsky net longwave flux at surface [W m^{-2}]
FLNS	Net longwave flux at surface [W m^{-2}]
RAIN	Atmospheric rain [mm s^{-1}]

Extended Data - Radiative forcing geoengineering increases Arctic temperature extremes and permafrost thawing

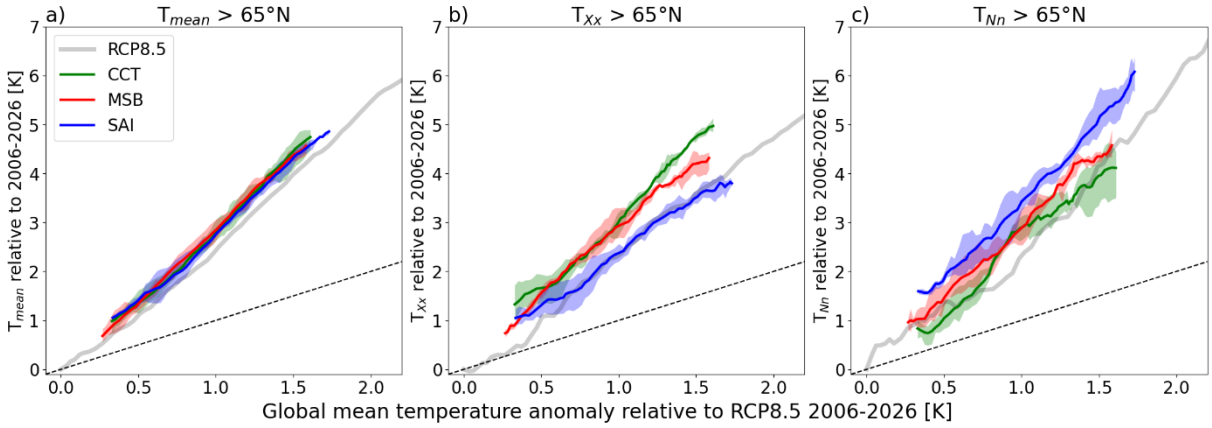

Extended Data Fig. 1: Simulated Arctic temperature change in RCP8.5, CCT, MSB and SAI. Anomaly in mean (T_{mean}), maximum (T_{Xx}) and minimum (T_{Nn}) land temperature north of 65°N compared to the global mean temperature anomaly over land and ocean (T_{glob}). The anomalies are respective to the mean of RCP8.5 from 2006-2026. The lines represent the ensemble mean. The ensemble spread is shaded. The hatched line represents the 1:1 line.

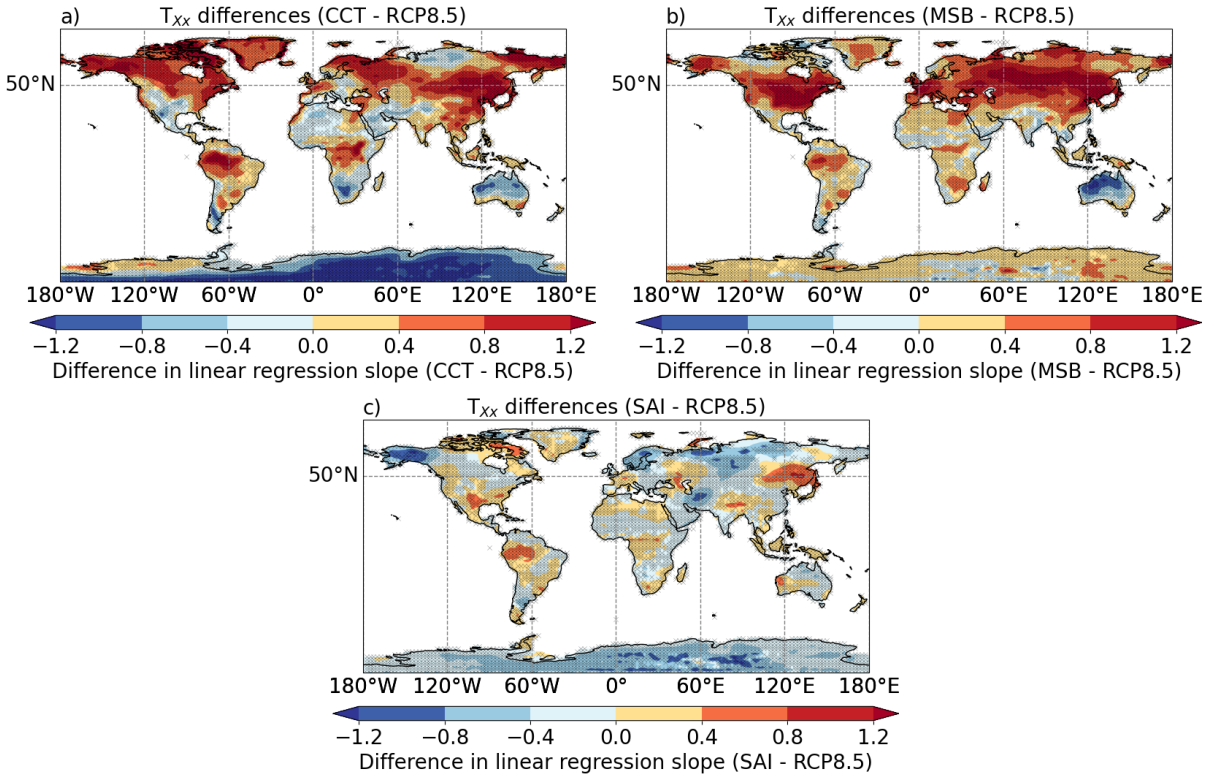

Extended Data Fig. 2: Simulated global change in T_{Xx} in CCT, MSB and SAI. Global pattern of the difference between the RCP8.5 and the RFG scenarios in the slope of the linear regression between T_{Xx} of each grid cell and the T_{glob}. Areas with a significant difference in slope of RCP8.5 and RFG scenarios are hatched.

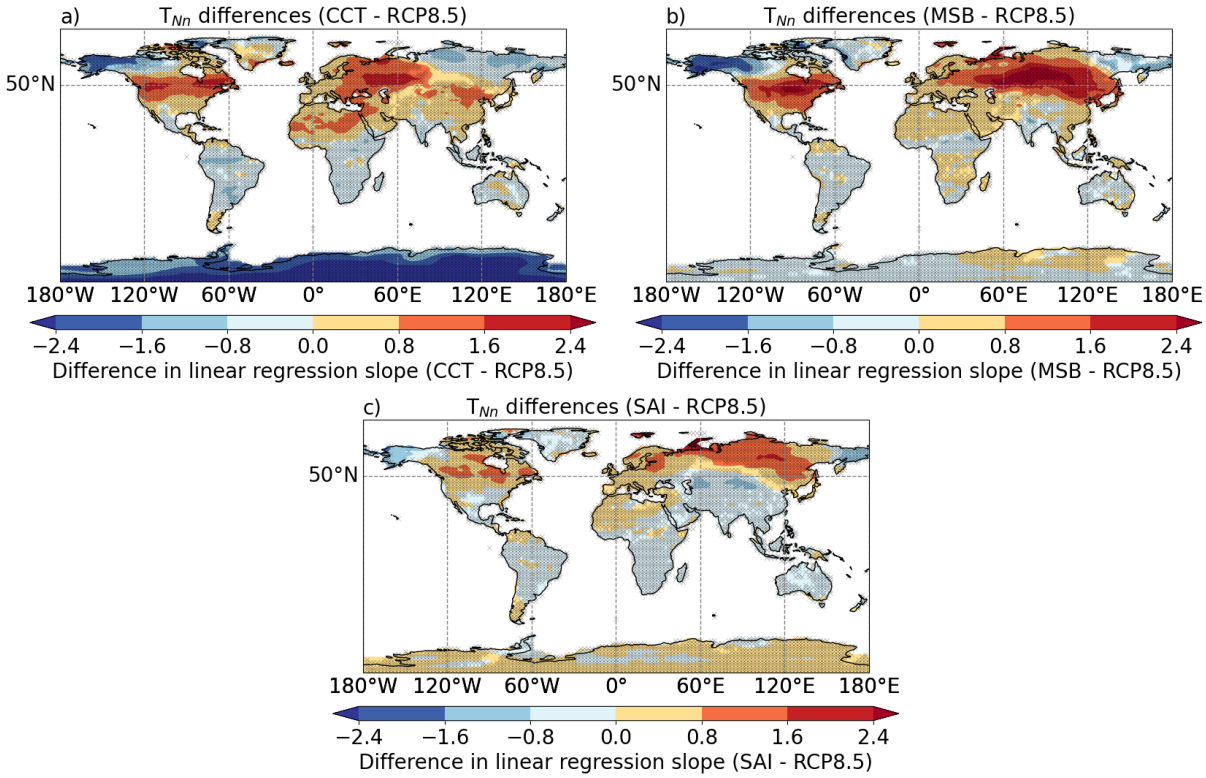

Extended Data Fig. 3: Simulated global change in T_{Nn} in CCT, MSB and SAI. Global pattern of the difference between the RCP8.5 and the RFG scenarios in the slope of the linear regression between T_{Nn} of each grid cell and the T_{glob}. Areas with a significant difference in slope of RCP8.5 and RFG scenarios are hatched.

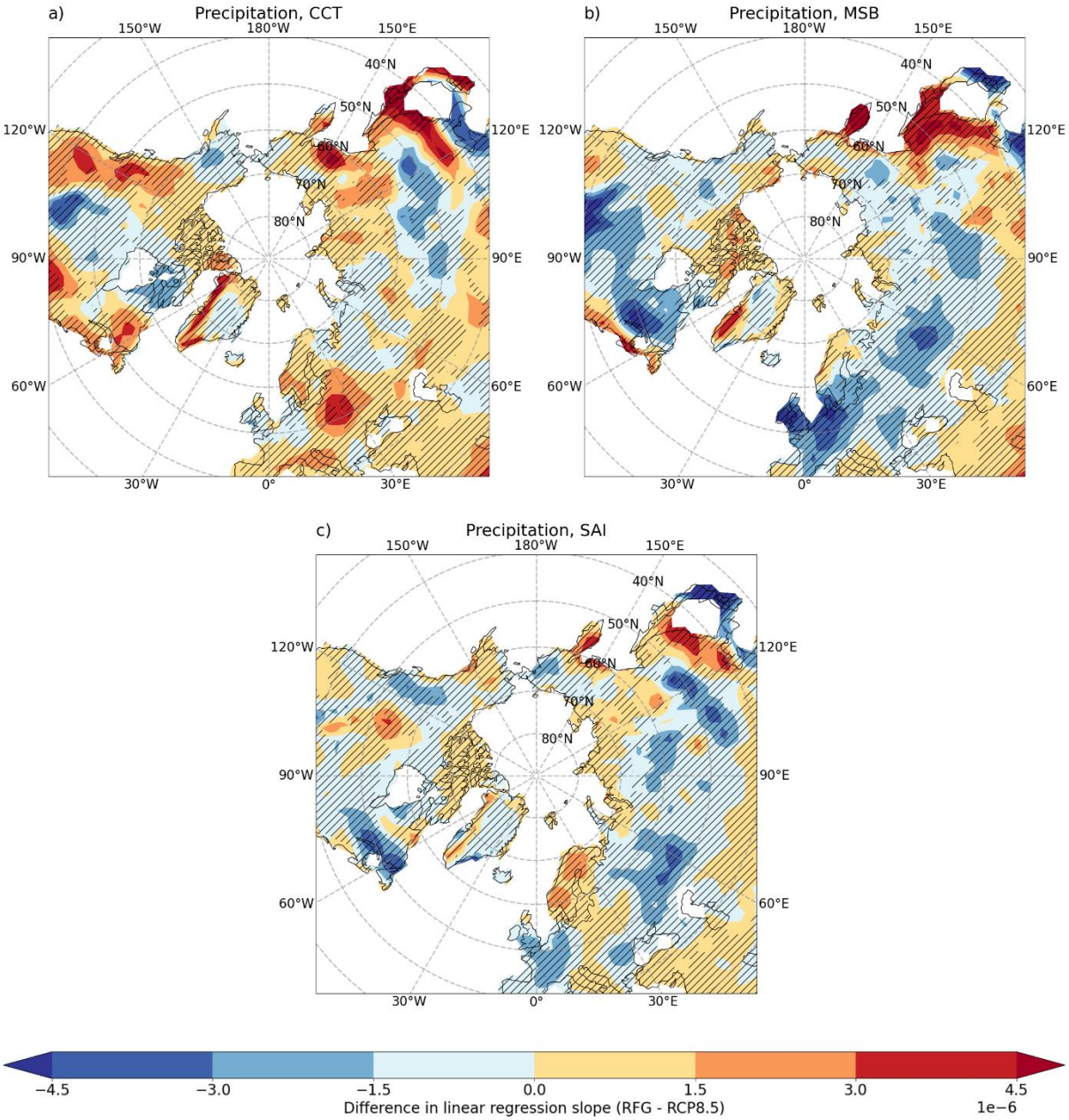

Extended Data Fig. 4: Simulated change of precipitation in the Arctic for CCT, MSB and SAI. Pattern of the difference between the respective RFG scenarios and the RCP8.5 scenario in the linear regression slope between precipitation and T_{glob}. Areas with a significant difference in slope of RCP8.5 and RFG scenarios are hatched.

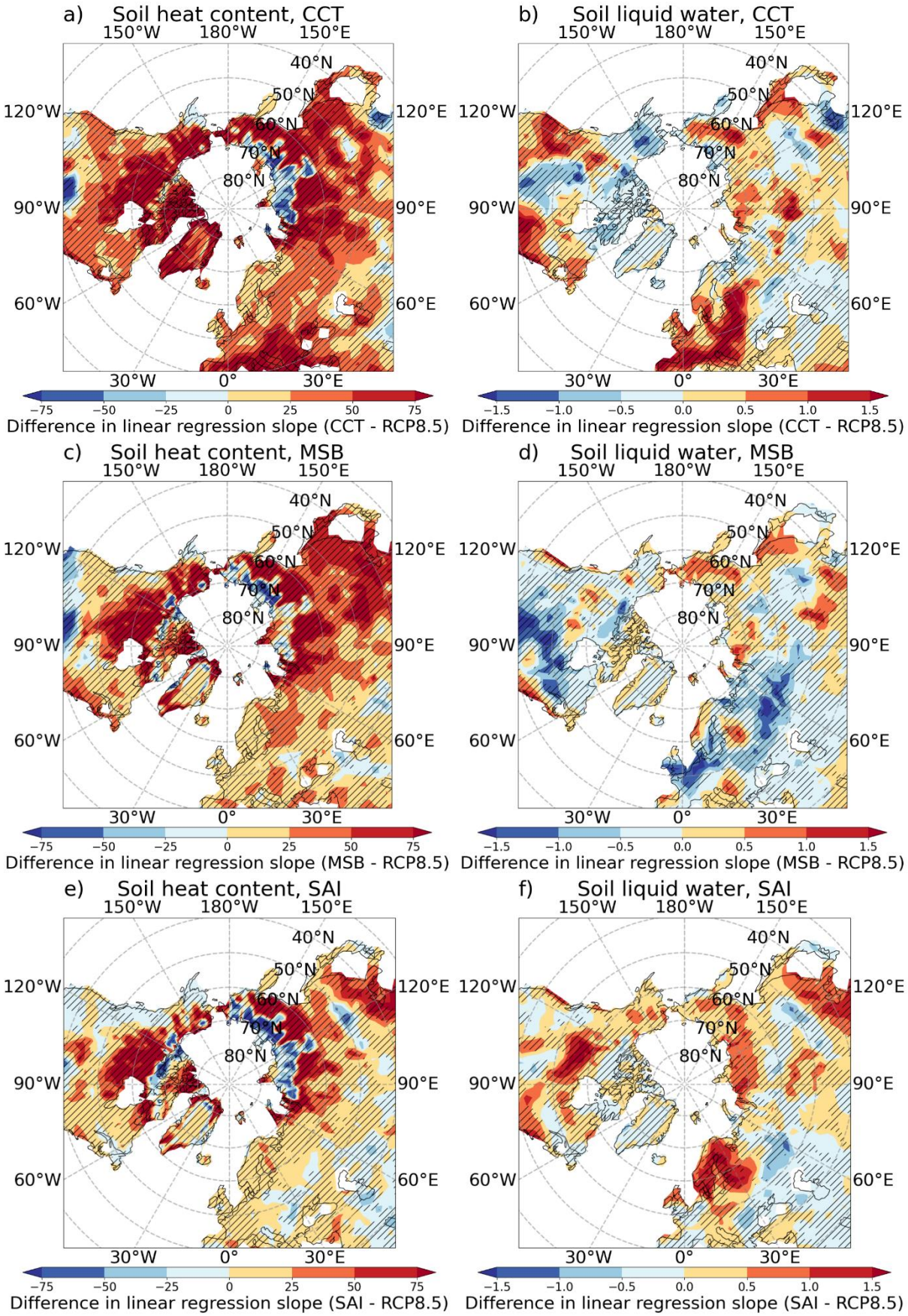

Extended Data Fig. 5: Simulated change of soil heat content and soil liquid water in the Arctic for CCT, MSB and SAI. Pattern of the difference between the respective RFG

scenarios and the RCP8.5 scenario in the linear regression slope between soil heat content and soil liquid water, respectively, and T_{glob}. Areas with a significant difference in slope of RCP8.5 and RFG scenarios are hatched.

Personal Declaration

Personal declaration: I hereby declare that the submitted Thesis is the result of my own, independent work. All external sources are explicitly acknowledged in the Thesis.

Uster, August 26 2022

Rhonda Müller